

Aus der Neurologische Klinik und Poliklinik  
Klinik der Ludwig-Maximilians-Universität

München

Vorstand: Prof. Dr. Marianne Dieterich

**EpCAM CAR T cells for the treatment of lung cancer brain metastasis-an in vivo  
imaging study in the mouse**

Dissertation

zum Erwerb des Doktorgrades der Medizin

an der Medizinischen Fakultät der

Ludwig-Maximilians-Universität zu München



vorgelegt von

Tao Xu

aus

Sichuan, P.R. China

2022

Mit Genehmigung der Medizinischen Fakultät  
der Universität München

Berichterstatter: Prof. Dr. Louisa von Baumgarten

Mitberichterstatter: Prof. Dr. Andreas Humpe  
Prof. Dr. Sebastian Kobold

Dekan: Prof. Dr. med. Thomas Gudermann

Tag der mündlichen Prüfung: 27.10.2022

## **Table of content**

<b>Table of content.....</b>	<b>1</b>
<b>Zusammenfassung (Deutsch).....</b>	<b>4</b>
<b>Abstract (English).....</b>	<b>7</b>
<b>List of figures.....</b>	<b>9</b>
<b>List of abbreviations.....</b>	<b>11</b>
<b>1. Introduction .....</b>	<b>14</b>
<b>1.1 Lung cancer brain metastasis (LCBM) .....</b>	<b>14</b>
<b>1.2 Chimeric antigen receptor (CAR) T cells.....</b>	<b>15</b>
<b>1.3 Epithelial cell adhesion molecules(EpCAM).....</b>	<b>18</b>
<b>1.4 Two-photon laser scanning microscopy (TPLSM) .....</b>	<b>19</b>
<b>1.5 Aims of this project .....</b>	<b>19</b>
<b>2. Materials and methods .....</b>	<b>21</b>
<b>2.1 Cell culture .....</b>	<b>21</b>
<b>2.2 Fluorescence activated cell sorting (FACS) and flow cytometry.....</b>	<b>23</b>
<b>2.3 CAR vector.....</b>	<b>24</b>
<b>2.4 Bacterial plasmid replication.....</b>	<b>25</b>
<b>2.5 Plasmid isolation.....</b>	<b>25</b>

<b>2.6 Production of retrovirus particles.....</b>	<b>26</b>
<b>2.7 Preparation of CD8 T cells.....</b>	<b>27</b>
<b>2.8 Retroviral T cell transduction.....</b>	<b>28</b>
<b>2.9 IFN-<math>\gamma</math> release assay.....</b>	<b>29</b>
<b>2.10 Mouse experiments.....</b>	<b>30</b>
<b>2.10.1 Mouse strain.....</b>	<b>30</b>
<b>2.10.2 Chronic cranial window implantation.....</b>	<b>31</b>
<b>2.10.3 Stereotactic injection of tumor cells and T cells.....</b>	<b>32</b>
<b>2.11 In vivo two-photon laser scanning microscopy (TPLSM).....</b>	<b>34</b>
<b>2.12 Image analysis.....</b>	<b>35</b>
<b>2.13 Statistical analysis.....</b>	<b>36</b>
<b>3. Results.....</b>	<b>37</b>
<b>3.1 Stable expression of tdTomato and EpCAM in LLC1.....</b>	<b>37</b>
<b>3.2 Establishment of the LCBM animal model.....</b>	<b>38</b>
<b>3.3 Visualization of LCBM growth in vivo.....</b>	<b>40</b>
<b>3.4 Transduction ratio of CAR T cells.....</b>	<b>41</b>
<b>3.5 IFN-<math>\gamma</math> release assay.....</b>	<b>41</b>
<b>3.6 In vivo dynamics of CAR T cells and untransduced T cells after intraparenchymal injection.....</b>	<b>42</b>

<b>3.7 Anti-tumor cytotoxicity, leading to tumor regression or inhibition.....</b>	<b>46</b>
<b>3.8 The distribution of intratumoral CAR T cells.....</b>	<b>48</b>
<b>3.9 The velocity of intratumoral CAR T cells.....</b>	<b>51</b>
<b>3.10 Blood sampling.....</b>	<b>53</b>
<b>3.11 Survival rates.....</b>	<b>53</b>
<b>4. Discussion.....</b>	<b>55</b>
<b>4.1 Mouse model.....</b>	<b>55</b>
<b>4.2 CAR T cells treatment.....</b>	<b>56</b>
<b>4.3 Recruitment of CAR T cells into solid tumor.....</b>	<b>57</b>
<b>4.4 The persistence of CAR T cells.....</b>	<b>58</b>
<b>4.5 Intratumoral CAR T cells velocity.....</b>	<b>59</b>
<b>4.6 Limitations .....</b>	<b>60</b>
<b>4.7 Clinical relevance.....</b>	<b>61</b>
<b>5. Conclusion.....</b>	<b>63</b>
<b>6. References.....</b>	<b>64</b>
<b>7. Acknowledgement.....</b>	<b>73</b>
<b>8. Affidavit.....</b>	<b>75</b>

## Zusammenfassung

Patienten mit Bronchialkarzinom weisen ein hohes Risiko auf im Verlauf ihrer Erkrankung Hirnmetastasen zu entwickeln. Dies ist mit einer nach wie vor infausten Prognose assoziiert. Daher ist es entscheidend, neue Therapiestrategien in der Behandlung von Hirnmetastasen zu identifizieren.

Chimäre Antigenrezeptor (CAR) T Zellen stellen einen Durchbruch in der zellbasierten Immuntherapie hämatologischer Malignome dar. Ihre therapeutische Wirksamkeit in der Behandlung von soliden Tumoren, insbesondere von Hirnmetastasen, bleibt jedoch unklar. Bislang war es nicht möglich, die therapeutische Wirksamkeit sowie biologische Charakteristika (Infiltration in Hirnmetastasen, zelluläre Interaktionen und Persistenz) im Zeitverlauf zu analysieren.

Um die therapeutische Effektivität einer Therapie mit CAR T Zellen in der Behandlung von Hirnmetastasen des Bronchialkarzinoms zu untersuchen, wurde im Rahmen der vorliegenden Arbeit daher ein syngenes, orthotopes, zerebrales Mausmodell zur *in vivo* Mikroskopie von Hirnmetastasen entwickelt. Durch die Kombination eines chronischen kranialen Fensters mit repetitiver *in vivo* Zwei-Photonen-Laser-Scanning-Mikroskopie wurde in diesem Mausmodell die therapeutische Effektivität sowie die Biologie von CAR T Zellen in der Behandlung von Hirnmetastasen des Bronchialkarzinoms auf zelluläre Ebene untersucht.

In einem ersten Schritt wurde ein syngenes, orthotopes Mausmodell etabliert. Hierfür wurde mittels Transfektion auf murinen Lewis-Lungenkarzinomzellen (LLC1) das epitheliale Zelladhäsionsmolekül (EpCAM) und ein rot fluoreszierendes Protein (tdTomato, tdT) stabil

exprimiert (EpCAM-LLC1-tdT). Nach mikrochirurgischer Präparation eines chronischen kraniellen Fensters wurden EpCAM-LLC1-tdT stereotaktisch in den Kortex von C57Bl6-Mäusen injiziert. Das Tumorwachstum wurde mittels repetitiver *in vivo* Zwei-Photonen-Laser-Scanning-Mikroskopie und post mortem immunhistochemisch charakterisiert.

In einem nächsten Schritt wurden gegen EpCAM gerichtete, grün fluoreszierende CAR T Zellen der zweiten Generation generiert und *in vitro* validiert. Zur Beurteilung ihrer therapeutischen Wirksamkeit und ihres biologischen Verhaltens *in vivo* wurden CAR T Zellen bzw. untransduzierte T Zellen in das angrenzende Hirnparenchym injiziert, nachdem sich solide EpCAM-LLC1-tdT Hirnmetastasen gebildet hatten.

Die Therapie mit CAR T Zellen führte in der Behandlungsgruppe zu einer Hemmung des Tumorwachstums und zu einem verbesserten Überleben. Bei 4 von 10 Mäusen (40 %) konnte eine vollständige Rückbildung etablierter Tumore beobachtet werden, während 6 von 10 Mäusen (60 %) eine deutliche Wachstumshemmung im Vergleich zu Tieren zeigten, die untransduzierte T Zellen erhielten. 1 von 8 Mäusen (12,5 %), denen die Injektion verabreicht wurde, zeigte jedoch auch eine Regression der etablierten Hirnmetastasen, was nahelegt, dass auch untransduzierte T Zellen eine anti-Tumor Aktivität aufweisen. Im Vergleich zu Kontrolltieren beobachteten wir eine erhebliche Anhäufung CAR T Zellen innerhalb des Tumors. Allerdings nahm die Zahl der CAR T Zellen im Tumor während des Beobachtungszeitraums deutlich ab, was auf eine unzureichende Persistenz hinweist.

Insgesamt, zeigen unsere Ergebnisse dass intrakraniell injizierte CAR T Zellen relevante

Antitumorwirkungen bei Hirnmetastasen des Bronchialkarzinoms hervorrufen können. Es scheint allerdings sinnvoll Strategien zur Verbesserung der intratumoralen Persistenz von CAR T Zellen in Hirnmetastasen zu identifizieren, um den Erfolg einer solchen Therapie weiter zu optimieren.

## **Abstract**

Lung cancer patients have a high risk for the development of brain metastases, which still have a dismal prognosis. Chimeric antigen receptor (CAR) T cells are a powerful class of cell-based immunotherapy for hematological malignancies. However, their therapeutic efficacy in the treatment of solid tumors, especially in brain metastasis remains unclear. In particular, the detailed cell dynamics of CAR T cell infiltration into brain metastasis, their intratumoral persistence as well as their therapeutic efficacy have not been studied in detail.

To address these aspects, we developed a syngeneic orthotopic cerebral metastasis model in mice. By combining a chronic cranial window with repetitive intracerebral two-photon laser scanning microscopy we aimed to characterize the treatment response as well as the biological behavior of CAR T in the treatment of lung cancer brain metastasis on a cellular level.

In a first step, a syngeneic orthotopic mouse model of large intracerebral lung cancer brain metastasis (LCBM) was established. Lewis lung carcinoma cells (LLC1) were transfected to express the epithelial cell adhesion molecule (EpCAM) and a red fluorescent protein (tdTomato, tdT). After microsurgical preparation of a cranial window preparation, EpCAM-LLC1-tdT were stereotactically injected into the cortex of C57Bl6 mice. Tumor growth was analyzed using repetitive TPLSM, furthermore, tumor growth was assessed by immunohistochemistry of excised brains. Tumor cells initially grew along preexisting intracerebral brain vessels which was then followed by the induction of extensive tumor angiogenesis. 11-17 days after tumor cell injection, we observed large LCBM with extensive pathologic vascularization, reflective of human brain metastasis of lung cancer.

In a next step, green fluorescent second-generation CAR T cells directed against EpCAM were generated and validated in vitro. To assess their therapeutic efficacy and biological behavior in vivo CAR T cells were injected into the adjacent brain parenchyma after solid brain metastasis of EpCAM-LLC1-tdT had formed.

Therapy with EpCAM-directed CAR T cells led to the inhibition of tumor growth in the treatment group and translated into an improved survival. Complete regression of established tumors could be observed in 4 of 10 mice (40%), while 6 of 10 mice (60%) showed a marked growth inhibition compared to animals receiving untransduced T cells. However, 1 of 8 mice (12.5%) injected also showed regression of established LCBM, suggesting potential anti-tumor activity of activated mock CAR T cells. Compared to controls treated with mock CAR T cells, we observed a substantial accumulation of CAR T cells within the tumor. However, the number of CAR T cells within the tumor markedly decreased during the observation period, pointing towards insufficient persistence of CAR T cells.

Collectively, our results demonstrate that CAR T cells injected into the cerebral parenchyma may induce relevant anti-tumor effects in LCBM. Strategies improving the intratumoral persistence of CAR T cells in brain metastases are warranted to further boost the success of such therapy.

## List of figures

<b>Figure 1   Computed tomography and magnetic resonance images of lung cancer brain metastasis.....</b>	<b>15</b>
<b>Figure 2   Illustration of the T cell receptor (TCR) and the second-generation chimeric antigen receptor (CAR).....</b>	<b>16</b>
<b>Figure 3   The ways of CAR T cells killing tumors.....</b>	<b>17</b>
<b>Figure 4   The schematic diagram of epithelial cell adhesion molecule located at the cell surface.....</b>	<b>18</b>
<b>Figure 5   pLVX-tdTomato-IRES-Neo plasmid.....</b>	<b>22</b>
<b>Figure 6   Murine EpCAM sequence was cloned into pMX plasmid.....</b>	<b>23</b>
<b>Figure 7  Vector for EpCAM CAR transduction.....</b>	<b>24</b>
<b>Figure 8   Cranial window implantation.....</b>	<b>32</b>
<b>Figure 9   Stereotactic injection of tumor cells and CAR T cells.....</b>	<b>33</b>
<b>Figure 10   In vivo two-photon laser scanning microscopy and the time frame of experiment.....</b>	<b>35</b>
<b>Figure 11   For the intensity of tdTomato fluorescence on transduced EpCAM-LLC1-tdT cells.....</b>	<b>37</b>
<b>Figure 12   For the expression ratio of EpCAM epitope on transduced EpCAM-LLC1-tdT cells.....</b>	<b>38</b>
<b>Figure 13   The status of microglia/macrophages after cranial window implantation.....</b>	<b>39</b>
<b>Figure 14   Visualization of intracerebral LCBM growth in vivo via two-photon microscopy.....</b>	<b>40</b>
<b>Figure 15   Transduction ratio of CAR EpCAM GFP plasmids.....</b>	<b>41</b>
<b>Figure 16   In vitro IFN-<math>\gamma</math> release assay.....</b>	<b>42</b>
<b>Figure 17   In vivo imaging of untransduced T Cells in orthotopic lung cancer brain metastasis.....</b>	<b>43</b>
<b>Figure 18   In vivo imaging of CAR T cells in orthotopic lung cancer brain metastasis.....</b>	<b>44</b>
<b>Figure 19   In vivo CAR T cell dynamics after intraparenchymal injection and tumor was inhibited.....</b>	<b>45</b>
<b>Figure 20   In vivo CAR T cell dynamics after intraparenchymal injection and tumor was eradicated.....</b>	<b>45</b>
<b>Figure 21   In vivo untransduced T cell dynamics after intraparenchymal</b>	

<b>injection and tumor unrestrictedly grew.....</b>	<b>46</b>
<b>Figure 22   Intracranial LCBM growth after injection of CAR T cells.....</b>	<b>47</b>
<b>Figure 23   Intracranial tumor growth of individual mouse after injection of CAR T cells.....</b>	<b>48</b>
<b>Figure 24   Intratumoral CAR T cell or untransduced T cell density.....</b>	<b>49</b>
<b>Figure 25   Intratumoral and contralateral CAR T cell density.....</b>	<b>50</b>
<b>Figure 26   Intratumoral and contralateral untransduced T cell density.....</b>	<b>51</b>
<b>Figure 27   Intratumoral CAR T cell and untransduced T cell velocity.....</b>	<b>52</b>
<b>Figure 28   Flow cytometry of CAR T cells and untransduced T cells in the peripheral blood.....</b>	<b>53</b>
<b>Figure 29   Survival rates after CAR T cells or untransduced T cells i.c. injection.....</b>	<b>54</b>

---

## List of abbreviations

**AF** Alexa fluor

**BBB** Blood brain barrier

**CAR** Chimeric antigen receptor

**CNS** Central nervous system

**CRS** Cytokine release syndrome

**CSF** Cerebrospinal fluid

**CTL** Cytotoxic T lymphocytes

**LBGM** Lung cancer brain metastasis

**DNA** Deoxyribonucleic acid

**DPBS** Dulbecco's phosphate-buffered saline

**FACS** Fluorescence-activated cell sorting

**FBS** Fetal bovine serum

**FELASA** Federation of european laboratory animal associations

**G418** Geneticin

**GFP** Green fluorescent protein

---

**i.p.** Intraperitoneal

**IRES** Internal ribosome entry site

**i.v.** Intravenous

**i.c.** Intracerebral

**LB** Lysogeny broth

**IFN- $\gamma$**  Interferon gamma

**MHC** Major histocompatibility complex

**MMF** Medetomidine/midazolam/fentanyl

**MRI** Magnetic resonance imaging

**CT** Computer tomography

**NaCl** Sodium chloride solution

**NOD** Non-obese diabetic

**PFA** Paraformaldehyde

**Plat-E** Platinum E, a retroviral packaging cell line

**PMT** Photo multiplier tube

**RFP** Red fluorescent protein

---

**ROI**      Region of interest

**rcf**      Relative centrifugal force

**s.c.**      Subcutaneous

**scFv**      Single chain variable fragment

**SCID**      Severe combined immunodeficiency

**s.e.m.**      Standard error of the mean

**SHG**      Second harmonic generation

**tdTomato**      Tandem dimer tomato, a red fluorescent protein derived from a monomeric mutant of DsRed

**TCR**      T cell receptor

**TILs**      Tumor infiltrating lymphocytes

**TPLSM**      Two-photon laser scanning microscopy

**Treg**      Regulatory T cell

**B-ALL**      B cell acute lymphoid leukemia

**DLBCL**      Diffuse large B cell lymphoma

---

## 1. Introduction

### 1.1 Lung cancer brain metastasis (LCBM)

Lung cancer is the second most common cancer and the leading cause of cancer death ([Bray et al., 2018](#), [Ferlay et al., 2019](#), [Siegel et al., 2020](#), [Sung et al., 2021](#)) with an overall 5-year survival rate of 20.5% ([Ramirez and Trapido, 2020](#)). Lung Cancer is the most common source of brain metastasis ([Pechoux et al., 2016](#), [Vargo, 2017](#), [Valiente et al., 2018](#), [Boire et al., 2020](#)), and 50% of lung cancer patients develop brain metastasis over the course of the disease (Figure 1). At present, the treatment of patients with brain metastases from lung cancer should be based on surgery, whole brain radiotherapy (WBRT), stereotactic radiotherapy (SRT), chemotherapy and molecular therapy for brain metastases ([Rusthoven et al., 2020](#), [Page et al., 2020](#)). However, median survival of lung cancer patients who develop brain metastasis ranges from 2.3-13.5 months ([Yousefi et al., 2017](#)). Given that therapeutic advances for lung cancer involving immunotherapeutic or targeted agents have resulted in prolonged disease courses, this number might increase in the next decades ([Fox et al., 2011](#), [Kalkanis and Linskey, 2010](#)). Although control of extracranial disease can often be achieved using such agents, a considerable number of patients succumb to their intracranial tumor.

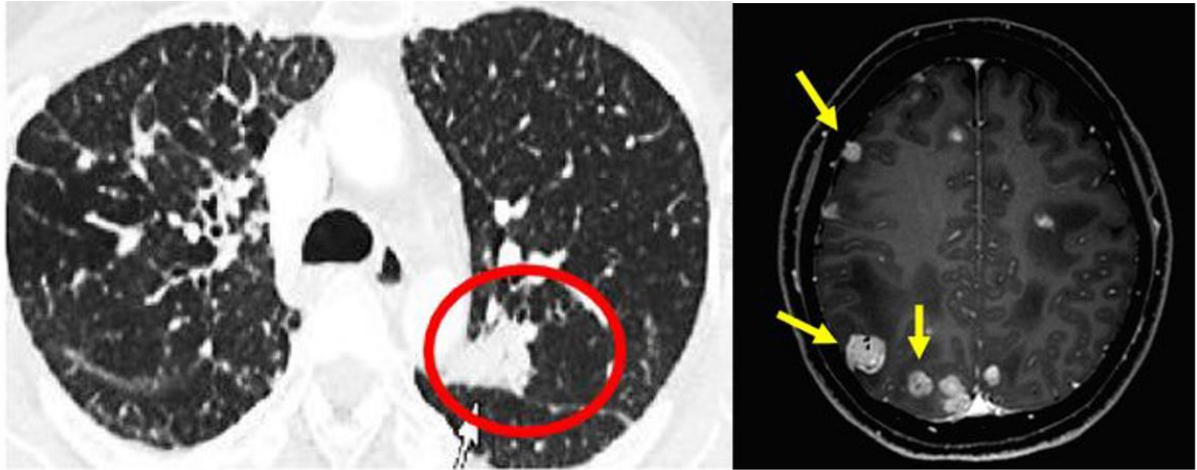


**Figure 1 | Computed tomography and magnetic resonance images of lung cancer brain metastasis ([Yun et al., 2020](#))**

Axial image of computed tomography scanning (left) displays a lesion of a primary lung cancer and axial image of magnetic resonance images (right) shows few lesions of lung cancer brain metastasis.

## 1.2 Chimeric antigen receptor (CAR) T cells

Chimeric antigen receptor (CAR) T cells are considered as one of the most successful breakthroughs in the area of tumor immunotherapy during the last decade ([Fesnak et al., 2016](#), [Yeku et al., 2017](#), [Bachanova et al., 2020](#), [Gauthier and Turtle, 2021](#)) Chimeric antigen receptors are genetically engineered proteins expressed on T cells. CARs typically include an extracellular domain and intracellular domain. The extracellular domain usually harbors a single-chain variable fragment as an extracellular ligand recognition domain providing tumor antigen specificity. The intracellular T cell activating domain includes a CD3 zeta chain, and, to ensure a more persistent CAR T cell activity, a co-stimulatory domain such as CD28 or 4-1BB ([Cheadle et al., 2014](#), [Toth et al., 2020](#), [Iragavarapu and Hildebrandt, 2021](#)).

Compared to traditional T cell receptor-based adoptive cell therapy, CAR T cells target tumor-specific surface antigens independent of major histocompatibility complex (MHC)

presentation ([Hartmann et al., 2017](#)), and have no limitation of self-antigen tolerance during the traditional T cell receptor-based adoptive cell therapy (Figure 2).

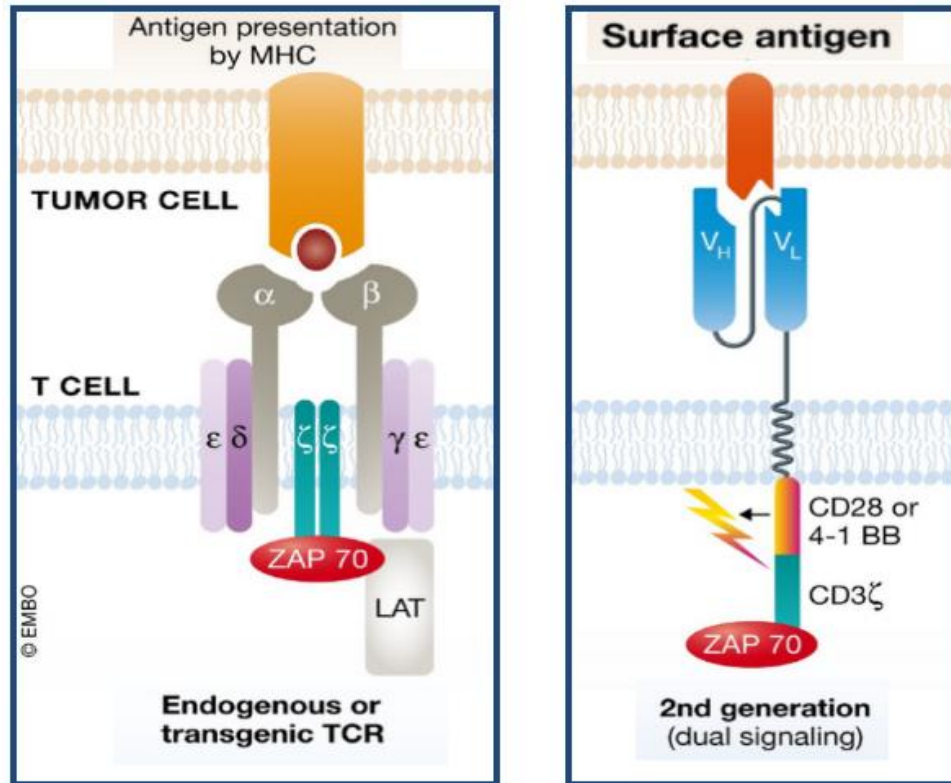


**Figure 2 | Illustration of the T cell receptor (TCR) and the second-generation chimeric antigen receptor ([Hartmann et al., 2017](#))**

The left picture displays T cell receptor. It depends on the antigen presentation of major histocompatibility complexes (MHC). In cancer, tumor cells frequently downregulate MHC expression as an immune escape mechanism. However, the chimeric antigen receptor (right picture) has an extracellular ligand binding domain, and it consists of single-chain variable fragments derived from immunoglobulin domains. Therefore, chimeric antigen receptor activation does not depend on MHC presentation and CAR T cells can perform its cytotoxicity function against tumor cells (Adopted from Jessica Hartmann, 2017).

CAR T Cells mediate tumor killing via three axes in solid tumors ([Benmebarek et al., 2019](#), [Upadhyay et al., 2021](#)). First, CAR T cells utilize the granzyme and perforin axis for effective and specific lysis of the antigen positive tumor cells. Second, CAR T cell derived cytokines can sensitize the tumor stroma. Driving IFN- $\gamma$  receptor up-regulation, thereby facilitating

stromal cell targeting by IFN- $\gamma$ . Third, within an antigen positive milieu, the antigen negative fraction can be targeted by CAR T cells via Fas and Fas L axis. Fas L is a member of the tumor necrosis factor family. The combination of Fas L on CAR T cells and Fas on tumor cells induces apoptosis of Fas positive tumor cells (Figure 3).

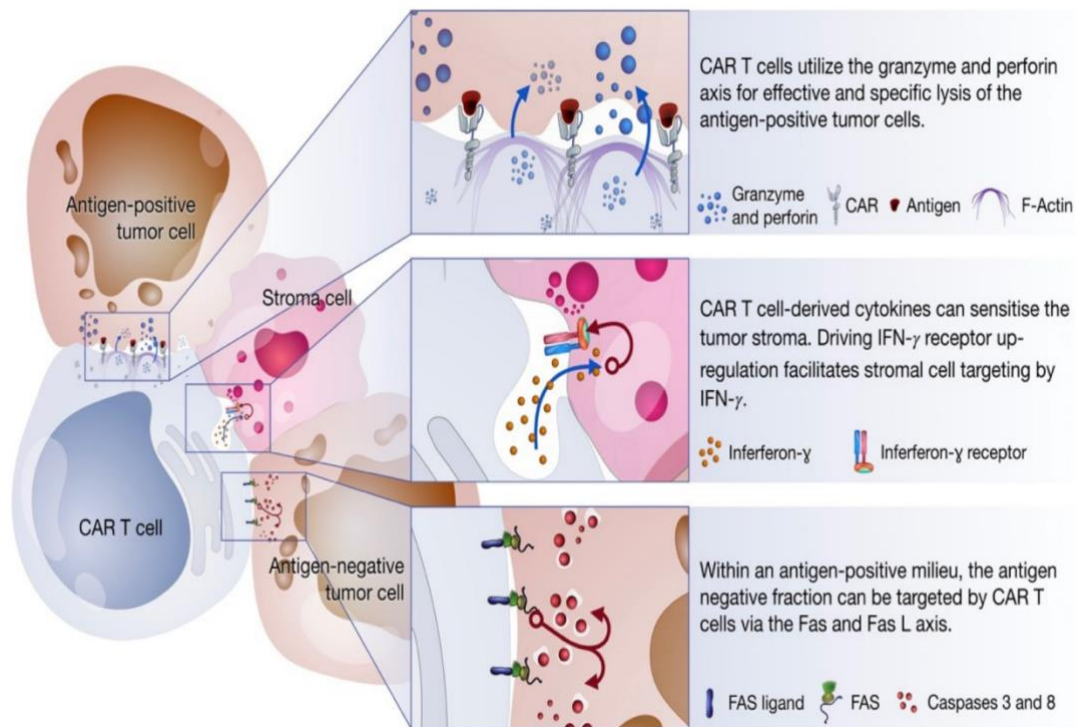


**Figure 3 | The ways of CAR T cells killing tumors (Benmebarek et al., 2019)**

The schematic diagram respectively introduces three axes of CAR T cells mediating tumor killing in solid tumor (Adopted from Benmebarek MR. 2019).

Due to the high response rate, CAR T cells directed against the pan B cell antigen CD19 were approved by FDA and EMA for treating patients with refractory B cell malignancies like acute lymphoid leukemia (B-ALL) and diffuse large B cell lymphoma (DLBCL) in 2017 and 2018 respectively (Jorgensen et al, 2020). Substantial efforts to translate such therapy into therapy for solid tumors, including primary as well as secondary brain tumors have been made. First preclinical and also clinical data show, that CAR T cells may hold therapeutic

---

efficacy for the treatment of lung cancer ([Li et al., 2018](#), [Wallstabe et al., 2019](#), [Feng et al., 2016](#), [Reppel et al., 2022](#)). However, it remains elusive, whether CAR T cells can be used to treat LCBM.

### **1.3 Epithelial cell adhesion molecules (EpCAM)**

The epithelial cell adhesion molecule is located at the cell surface (Figure 4). It is a transmembrane glycoprotein which can mediate epithelial specific intercellular adhesion ([Moldenhauer et al., 2012](#), [Kim et al., 2019](#), [Moin et al., 2021](#)). It is overexpressed on multiple types of lung cancer cells ([Patriarca et al., 2012](#), [Iyer et al., 2013](#), [Miao et al., 2022](#)). It is involved in cell signaling, proliferation, adhesion and migration properties of cancer cells ([Trzpis et al., 2007](#), [Simon et al., 2013](#), [Yang et al., 2020](#), [Williams et al., 2021](#)). EpCAM is overexpressed in about 50% of non-small cell lung cancer ([Kim et al., 2009](#)). Its overexpression is typically also conserved in metastatic disease ([Spizzo et al., 2011](#)) and in some cancers even upregulated in metastases compared to primary tumors ([Li et al., 2021](#)).

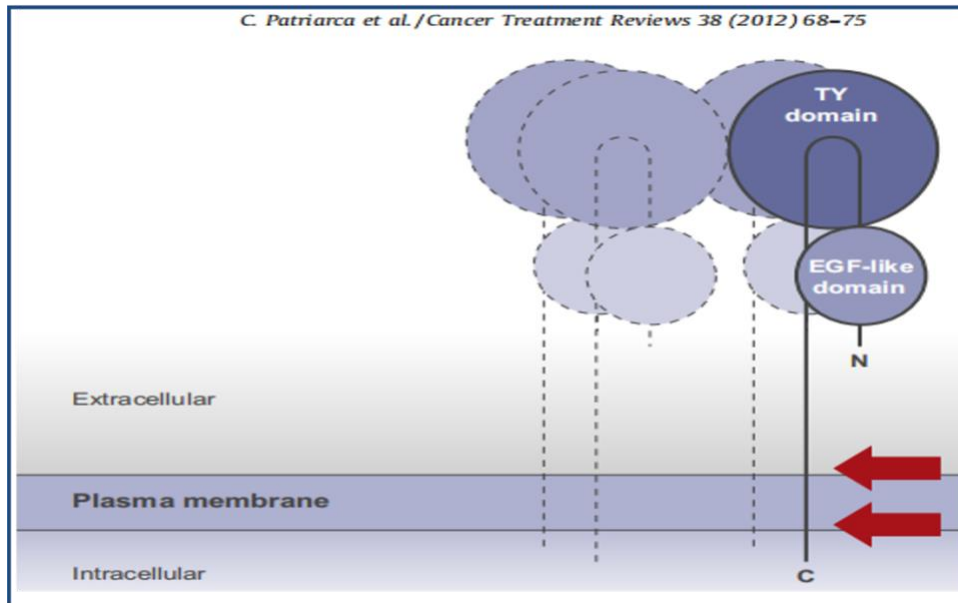


**Figure 4 | The schematic diagram of epithelial cell adhesion molecule located at the cell surface ([Patriarca et al., 2012](#))**

#### **1.4 Two-photon laser scanning microscopy (TPLSM)**

Both fluorescent microscopy and two-photon laser scanning microscopy (TPLSM) can image brain in living animals directly and repeatedly ([Hong et al., 2014](#)). During TPLSM two photons are absorbed into an excited state by a single fluorophore molecule. Compared to conventional fluorescent microscopy, two-photon laser scanning microscope has the advantage of a lower phototoxicity and photobleaching ([Nguyen et al., 2001](#), [Reshak, 2008](#)). TPLSM can be used to image the mouse brain for a long period of time than confocal fluorescent microscope. In addition, TPLSM is characterized by a deep tissue penetration ([Reshak, 2009](#)). TPLSM can be used to perform time lapse and 3D deep tissue imaging which can be reconstructed by computer and help researcher better understand the kinetic characteristics of CAR T cells at a cellular and even subcellular resolution ([Grimm et al., 2015](#), [Zipfel et al., 2003](#)). TPLSM allows to analyze complex interactions between tumor cells

---

and immune cells inside the living mouse brain ([Misgeld and Kerschensteiner, 2006](#), [Kobat et al., 2009](#), [Horton and Dworkin, 2013](#)).

### **1.5 Aims of this project**

Although the FDA has approved CAR T cells for clinical hematological tumors, it is still in the research stage for solid tumors. For patients with highly malignant lung cancer brain metastases who have lost the chance of surgical resection, CAR T cells may be a promising and novel treatment.

Therefore, the aims of this thesis are:

- a) to create a mouse animal model of lung cancer brain metastasis,
- b) to combine the mouse implanted chronic cranial window and long term in vivo TPLSM to track the in situ growth of lung cancer brain metastasis,
- c) to test the therapeutic efficacy of CAR T cells in a clinically relevant mouse model of lung cancer brain metastasis,
- d) to analyze CAR T cells recruitment, migration and persistence on a cellular resolution over time.

---

## 2. Materials and methods

### 2.1 Cell culture

Lewis lung carcinoma (LLC1) cells were purchased from ECACC (European Collection of Authenticated Cell Cultures, Catalog No. 90020104). The cells were grown in complete growth medium including Dulbecco's Modified Eagle' Medium (DMEM, Gibco, Catalog No. 41965-039) and Fetal Bovine Serum (FBS, Biochrom GmbH, Catalog No. S 0615) with a final 10% concentration. A PCR product containing the sequence of tdTomato (vector ptdTomato; #63-2531, TaKaRa Clontech) was cloned into the lentiviral expression vector pLVX-IRES-neo (LentiX-Bicistronic Expression System; #63-2181, TaKaRa Clontech) to generate a pLVX-tdTomato-IRES-Neo construct (Figure 5) ([Zhang et al., 2021](#)). Notably, a resistance-sequence for G418-sulfate is contained in the lentiviral expression vector. The resulting nucleotide pLVX-tdTomato-IRES-Neo was verified by Sanger sequencing and restriction enzyme digestion. LLC1 were transfected with pLVX-tdTomato-IRES-Neo using Lipofectamine (Lipofectamine 2000; Thermo Fisher Scientific). LLC1-tdT were enriched by cultivation in selection medium containing G418-sulfate (#A2912; Biochrom), and by repetitive FACS sorting. As previously described in detail ([Karches et al., 2019](#)), LLC1-tdT cells were stably transduced with a pMXs vector containing the full-length murine EpCAM (UNIPROT entry: #Q99JW5) cDNA to generate the EpCAM overexpressing cell line EpCAM-LLC1-tdT (Figure 6). Before transfecting LLC1, both of pLVX-tdTomato-IRES-Neo plasmid and pMX-EpCAM plasmid were sequenced to confirm. LLC1-tdT cells and EpCAM-LLC1-tdT cells were cultured in DMEM, 10% FBS and G418 (an aminoglycoside antibiotic, Biochrom GmbH, Catalog No. A 2912) with a 1000 µg/ml final concentration.

---

Subculture the cells at a ratio of 1:8 to 1: 10 every 3-4 days. Cells were resuspended by 2 ml of Trypsin (Biochrom GmbH, Catalog No. L 2123) during subculture. Cells were frozen in the medium containing 90% FBS, supplemented with 10% Dimethyl Sulfoxide (DMSO, SIGMA, Catalog No. D 2650). Long time storage was performed by keeping cells in liquid nitrogen vapor phase. PCR Mycoplasma Test Kit (PanReac AppliChem GmbH, Darmstadt, Germany) were regularly used to judge whether the cells are healthy. We culture the cells for a maximum period of 1 month to control the genetic drift to minimum.

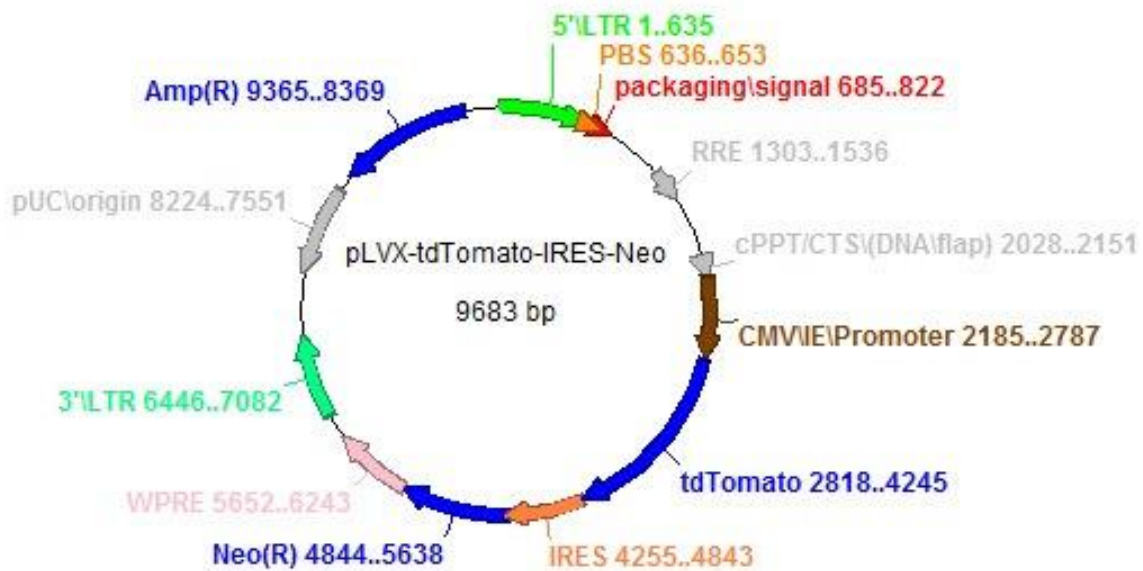


**Figure 5 | pLVX-tdTomato-IRES-Neo plasmid**

tdTomato sequence was cloned into a plasmid under CMV/IE/Promoter as described previously ([Zhang et al., 2021](#))

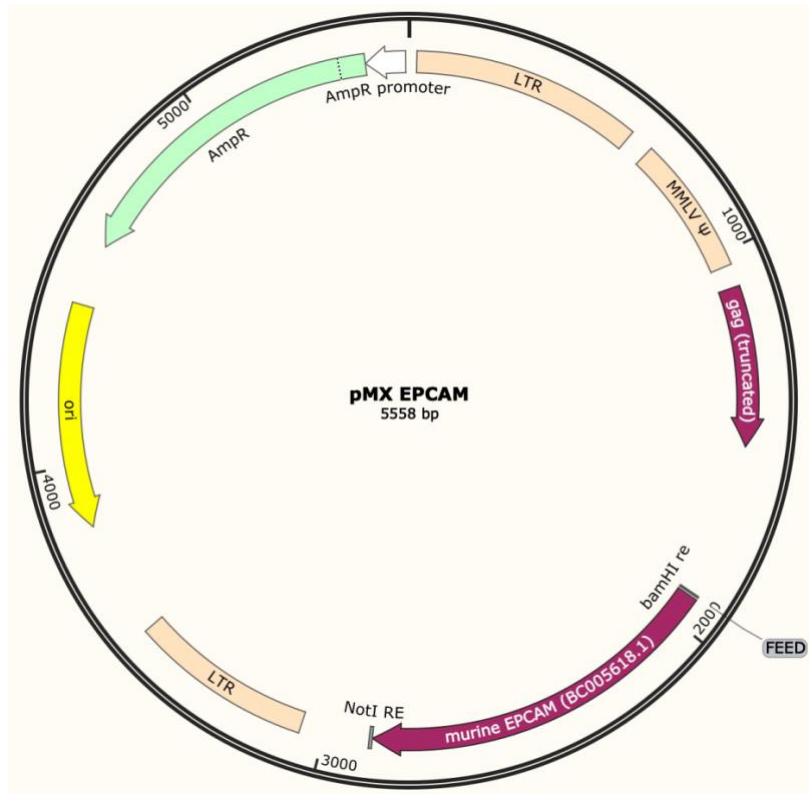


**Figure 6 | Murine EpCAM sequence was cloned into pMX plasmid ([Cadilha et al., 2021](#))**

## 2.2 Fluorescence activated cell sorting (FACS) and flow cytometry

Tumor cells with strong and homogeneous expression of tdTomato and EpCAM epitope were selected using FACS sorting. For FACS, tumor cells were suspended in 2 ml trypsin solution. After centrifugation, the supernatant was discarded and the cells were diluted in 1 ml of FACS buffer (10 ml PBS, Biochrom Cat. No. L1815; 40  $\mu$ l EDTA SIGMA, Cat. No. E8008-100ML; and 0.05g BSA, ROTH, Cat. No. 7365-45-9), and adjusted the concentration of tumor cells to  $1 \times 10^6$  in 100  $\mu$ l. Tumor cells were stained with Alexa Fluor® 647 anti-mouse CD326 (EpCAM) Antibody (BioLegend, Catalog No. 118212). A dosage of the antibody of  $\leq 0.25$   $\mu$ g per  $10^6$  cells in 100  $\mu$ l volume was used. After centrifugation, cells were diluted in FACS

---

buffer and the final concentration of is  $1-5 \times 10^6$ /ml tumor cells. Tumor cells were filtered to exclude cell clusters (Sysmex, Catalog No. 04-004-2326). A flow cytometry machine (BD LSRFortessa™ Cell Analyzer, Catalog No. 647794) and a cell sorting machine (MoFlo Astrios EQ, Cell Sorter, Beckman Coulter, Serial No.AT13011) were used, respectively.

### 2.3 CAR vector

In our study, we used a murine second-generation CAR which can specifically recognize EpCAM expressed on the surface of tumor cells. The CAR vector was kindly provided by our collaborator Prof. Sebastian Kobold (Division of Clinical Pharmacology, Faculty of Medicine, LUM, Munich, Germany). The anti-EpCAM-CAR construct was previously described by Lesch & Blumenberg et al. ([Lesch et al., 2021](#)) and consists of a single chain variable fragment that recognizes the murine EpCAM antigen (clone G8.8), fused to the transmembrane and signaling domains of murine CD28 and murine CD3zeta in a pMP71 backbone. The anti-EpCAM-CAR-GFP construct consists of anti-EpCAM-CAR fused to GFP via a self-cleaving 2A sequence (Figure 7). GFP-expressing, EpCAM directed CAR T cells (CAR T cells) were generated; and T cells transduced by a vector containing GFP only were used as controls (Untransduced T cells).



#### Figure 7 | Vector for EpCAM CAR transduction

The anti-mouse EpCAM scFv is fused to the CD8 derived hinge and transmembrane domains, then connect the CD28 costimulatory domain and the CD3ζ intracellular signaling domain. The green fluorescent protein sequence was used for assessing the transduction efficacy and

---

isolating CAR T cells.

## **2.4 Bacterial plasmid replication**

For plasmids replication, MAX Efficiency™ DH5αF'1Q competent Cells (Thermo Fisher, Catalog No. 18288019) were used. 50 ng of pMP71 plasmids containing EpCAM-CAR-GFP or GFP sequence were added to a volume of 100 µl of competent bacteria and incubated for 30 minutes. Afterwards the mixture was heated on the thermoshaker for 45 seconds at 42°C. In a next step, lysogeny broth (LB) medium (Sigma-Aldrich, Catalog No. L3397) was added to a total volume of 1 ml and incubated for 1 hour at 37°C at 200 rpm. One hour later, 100 µl of the transformed bacteria solution was distributed on the plate containing LB broth with agar (Sigma-Aldrich, Catalog No. L3147). The concentration of ampicillin (Sigma-Aldrich, Catalog No. A5354) inside the medium was 100 µg/ml. In order to expand the transformed bacteria, single colonies of bacteria were picked from the plate, and were grown in 10 ml of LB medium overnight at 37°C on a platform shaker with 200 rpm. On the second day, 2 ml of bacteria suspension was added to 200 ml of LB medium (200 ml double deionized water, 3.1 g LB powder) and was kept overnight at 37°C on a platform shaker with 200 rpm.

## **2.5 Plasmid isolation**

The EndoFree Plasmid Maxi Kit (QIAGEN, Catalog No. 12362) was used to isolate the desired plasmids according to manufacturer's instructions. Briefly, the expanded bacteria from overnight LB culture were harvested by centrifuging. The cell membrane was lysed with an alkaline solution and RNA was enzymatically removed from the lysate using RNase

---

solution provided in the kit. Endotoxin was removed and the plasmid was precipitated. After purification of the plasmid, the purity was measured by a spectrophotometer following the manufacturer's instructions (Thermo Scientific™ NanoDrop™ 2000/2000c, Catalog No.: ND 2000). If the ratio of absorbance at wavelengths of 260 nm and 280 nm (A<sub>260</sub>/A<sub>280</sub>) was more than 1.8, the purity of plasmid was considered good enough for further experiments.

## **2.6 Production of retrovirus particles**

To produce retrovirus, Platinum-E (Plat-E) Retroviral Packaging Cell Line (Cell Biolabs, Inc. Catalog No. RV-101) was transfected with the pMP71 plasmid using Lipofectamine 2000 transfection reagent (Thermo Fisher Scientific, Catalog No. 11668030). Briefly, on the first day, Plat-E cells were seeded in 6-well plate at a density of  $1 \times 10^6$  cells per well in DMEM medium supplemented with 10% FBS, 1% P/S (Thermo Fisher, Catalog No. 15140122). On the second day, Plat-E cells were transfected with Lipofectamine 2000 for 4 hours. Briefly, 15  $\mu$ g of plasmid was diluted with Opti-MEM (Thermo Fisher, Catalog No. 31985062) to a total volume of 150  $\mu$ l. 15  $\mu$ l of Lipofectamine 2000 was diluted with Opti-MEM to a total volume of 150  $\mu$ l. DNA solution was added into Lipofectamine 2000 solution dropwise while continuously vortex. During 20 minutes of incubation, complete DMEM medium was replaced with 700  $\mu$ l Opti-MEM. Then the DNA and Lipofectamine 2000 mixture was added into a 6 well plate dropwise and incubated for 4 hours. Afterwards, the transfection medium was replaced by 3 ml of complete DMEM medium. The supernatant from Plat-E cells which contained the retroviral particles was collected 24 hours and 48 hours after transfection and

---

was filtered through a 0.45µm Millex-HA Filter (Merck, Catalog No. SLHA033SB). The supernatant was immediately used to transduce primary mouse T cells.

## **2.7 Preparation of CD8 T cells**

One day before transduction, spleens of wild type C57Bl6 mice were isolated, meshed through a 30 µm MACS Smart Strainer (Miltenyi Biotec, 130-098-458) and placed in a 50 ml Falcon tube. The filter was rinsed two times with 10 ml murine T Cell Medium (mTCM) containing RPMI 1640 Medium Supplemented with GlutaMAX™ (Gibco™, Catalog No. 61870036), 10%FBS, 1%P/S, 1% Sodium Pyruvate (Thermo Fisher Scientific, Catalog No.#11360070) and 0,1% HEPES (Thermo Fisher Scientific, Catalog No.#15630056). The filtrate was centrifuged at 400 rcf for 5 minutes. The supernatant was discarded and the cell pellet was resuspended in 2 ml red blood cell lysis buffer (Thermo Fisher Scientific, Catalog No. 00-4333-57). After 2 minutes, 20 ml PBS was added and centrifuged at 400 rcf for 5 minutes. The cell pellet was resuspended in 5 ml mTCM. CD8 positive T cells were isolated with the mouse CD8a+ T Cell Isolation Kit according to the instructions of the manufacturer (Miltenyi Biotec, CAatlog No. 130-104-075). Briefly, 10 million cells were suspended in 40 µl of buffer (PBS, 0.5% BSA and 2mM EDTA). 10 µl of Biotin-Antibody Cocktail was added. The cells were mixed well and were incubate for 5 minutes at 4°C. Then 30 µl of buffer and 20 µl of Anti-Biotin Microbeads per 10 million cells were added, mixed and incubated for 10 minutes at 4 °C. Afterwards the LS Column (Miltenyi Biotec, Catalog No. 130-042-401) was put in the magnetic field of a MidiMACS Separator (Miltenyi Biotec, Catalog No.

---

130-042-302). The LS column was prepared by rinsing with 3 ml of buffer and the cell suspension was pipetted to the LS column. The flow-through which contained the enriched CD8 T cells was collected, washed and resuspended in mTCM, complemented with 25 IU/ml of IL-2 (Recombinant Human IL-2, cross reactive with mouse, Peprotech, Catalog No. 200-02), anti-mouse CD3 $\epsilon$  antibody (1:1000, clone 145-2C11, Thermo Fisher, Catalog No. 16-0031-86), anti-mouse CD28 antibody (1:10 000, clone 37.51, Thermo Fisher, Catalog No. 16-0281-86) and 2-Mercaptoethanol (1:1000, Gibco™, Catalog No. 21985023). The cells were stimulated overnight in 6 well plate. A non-tissue culture-treated 24 well plate (Life Sciences, Catalog No. 351147) was coated with 400  $\mu$ l per well of 12,5  $\mu$ g/ml RetroNectin solution (TaKaRa, Catalog No. T100B), and covered with sealing film (Merck, Catalog No. BR701624). and incubated overnight at 4°C.

## **2.8 Retroviral T cell transduction**

The supernatant was removed gently from the 24 well plate coated with RetroNectin and 500  $\mu$ l of blocking buffer (2% BSA, ddH<sub>2</sub>O and Albumin Fraction V) per well was added and incubated at 37°C for 30 minutes. The supernatant containing retrovirus from the Plat-E cells was carefully collected without detaching the Plat-E cells from plate. To collect retrovirus supernatant again after 24 hours, 3 ml of mTCM was added to the Plat-E cells and incubated with the cells overnight at 37 °C. The retrovirus supernatant was filtered with a Millex HA 0.45  $\mu$ m filter (Merck, Catalog No. SLHA033SB) and concentrated three times. Afterwards, the blocking buffer was replaced with 1 ml of washing buffer (0.025 Molarity HEPES in PBS).

---

1 ml concentrated retrovirus was transferred to the 24 well plate and centrifuged at 3000 rcf at 4 °C for 2 hours. CD8 T cells were adjusted at a cell concentration of 1 million cells per ml mTCM supplemented with 25 IU/ml of IL-2, and 2-Mercaptoethanol, and 10 µl of Dynabeads™ (Mouse T-Activator CD3/CD28 for T-Cell Expansion and Activation, Thermo Fisher Scientific, Catalog No. 11452D). The retrovirus supernatant was removed and 1 ml of cell suspension was added to the 24 well plate, centrifuge at 800 rcf at 32° C for 30 minutes and was incubated overnight at 37° C. On the second day, the retrovirus supernatant was collected again and 1 ml concentrated retrovirus solution was added per well, centrifuged at 800 rcf at 32° C for 90 minutes. On third day, the transduction efficiency was checked by flow cytometry (BD LSRFortessa™ Cell Analyzer, Catalog No. 647794). The cells expressing GFP signal were sorted on cell sorter (MoFlo Astrios EQ, Beckman Coulter, Catalog No. AT13011) for in vitro or in vivo experiments.

## **2.9 IFN-γ release assay**

20 000 tumor cells and 200 000 CAR T cells or untransduced T cells were seeded in the each well of a 96 well plate in a total volume of 200 µl culture medium (DMEM supplemented with 10%FBS, 1%L-GLU and 1%P/S) per well. 24 hours later, the content of the wells was transferred into a round bottom 96 well plate and spined down at 500 rcf for 5 minutes. 150 µl of co-culture supernatant was transferred to a new 96 well plate. Mouse IFN-γ ELISA Set (BD OptEIA™, Cat. No. 555138) was used to measure the IFN-γ release amount from co-culture cells according to the instructions of the manufacturer. Briefly 100 µl diluted

---

capture antibody was pipetted to each well of 96 well Nunc-Immuno™ polystyrene Maxisorp ELISA flat bottom plate (Thermo Fisher Scientific Cat. No. 442404) and incubated overnight at 4°C. The wells were aspirated and washed 5 times with  $\geq 300$   $\mu$ l/well wash buffer. Afterwards, the plates were blocked with 200  $\mu$ l assay diluent per well. After 1 hour of incubation at room temperature, the blocking diluent was aspirated and the plates were washed 5 times. 100  $\mu$ l sample was added to each well and incubated 2 hours at room temperature. Then the wells were aspirated and washed 5 times again. 100  $\mu$ l working detector (detection antibody + SAV-HRP) was added to each well. After 1 hour of incubation at room temperature the working detector was aspirated and the wells were washed 10 times. 100  $\mu$ l substrate solution was transferred to each well. After half an hour incubation at room temperature in dark 50  $\mu$ l stop solution was pipetted into each well. The absorbance was measured at 450 nm using a microplate reader, (Tecan GENios, F129004, Austria)

## **2.10 Mouse experiments**

All animal experiments were conducted followed the animal welfare act and the Bavarian state regulations for animal experiment. Protocols of all animal surgeries were approved by the local authorities.

### **2.10.1 Mouse strain**

To assess inflammation after chronic cranial window implantation, transgenic CX3CR1<sup>GFP/WT</sup> (The Jackson Laboratory, Stock No. 005582) mice were implanted with a chronic cranial

---

window, and imaged regularly to confirm how long the activated microglia and macrophages need to recover. CX3CR1<sup>GFP/WT</sup> mice have an enhanced GFP sequence replacing the first 390 bp of the coding exon (exon 2) of the chemokine (C-X3-C motif) receptor 1 (Cx3cr1) gene, microglia and macrophages has enhanced GFP which can be visualized under two-photon laser scanning microscope or epifluorescence microscope. For all other experiments male C57/BL6J mice (The Jackson Laboratory via their distributor, Charles River Germany, Stock No: 000664) were used. All mice were maintained at our facility according to Federation of European Laboratory Animal Associations guidelines. Experiments were started at the age of 8-14 weeks.

### **2.10.2 Chronic cranial window implantation**

Before surgical procedures, mice were anaesthetized using an intraperitoneal injection of 195 µl MMF (Midazolam (5 mg/kg, Pfizer, Karlsruhe, Germany), Fentanyl (0.05 mg/kg, CuraMed Pharma GmbH, Karlsruhe, Germany) and Medetomidine (0.5 mg/kg, Ratiopharm)). Microsurgical preparation of the cranial window was performed as previously described in detail ([Kienast et al., 2010](#), [von Baumgarten et al., 2011](#)). Briefly, the mouse head was fixed between two ear bars and one teeth bar in a stereotactic frame (David Kopf Instruments, Tujunga, USA), the chest and abdomen are on a heating pad. For preventing postoperative infection and brain edema, Cefotaxime (250 mg/kg, Fresenius Kabi Deutschland, Bad Homburg, Germany) and Dexamethasone (2mg/kg, Ratiopharm) were applied subcutaneously. The scalp was disinfected using povidone iodine solution (Braunol, B. Braun Melsungen AG).

---

The skin and the subcutaneous soft tissues were removed and a 5.5 mm circular part of the calvarium was removed using a sterile carbon steel micro dental drill (tip diameter: 0.5 mm, Fine Science Tools Germany, Heidelberg, Germany) and the dura was gently separated from the leptomeninges to achieve optimal image resolution. Sterile sponges containing thrombin and fibrinogen (TachoSil, Takeda Austria, Linz, Austria) was used to stop eventual bleeding. The cortical surface was covered with saline, and a sterile round cover glass (diameter: 6 mm) was attached to the cranium using dental glue (Cyano veneer, Hager Werken, Duisburg, Germany). To facilitate optimal head positioning during imaging, a custom-made plastic ring (diameter: 8 mm) was also glued to the skull (Figure 8). Buprenorphine (0.1 mg/kg; every 8 hours) was injected for two postoperative days to ensure analgesia. Prior to further experiments, a postoperative recovery time of 28 days was granted to prevent postoperative inflammation or alterations of the microcirculation from affecting our results.

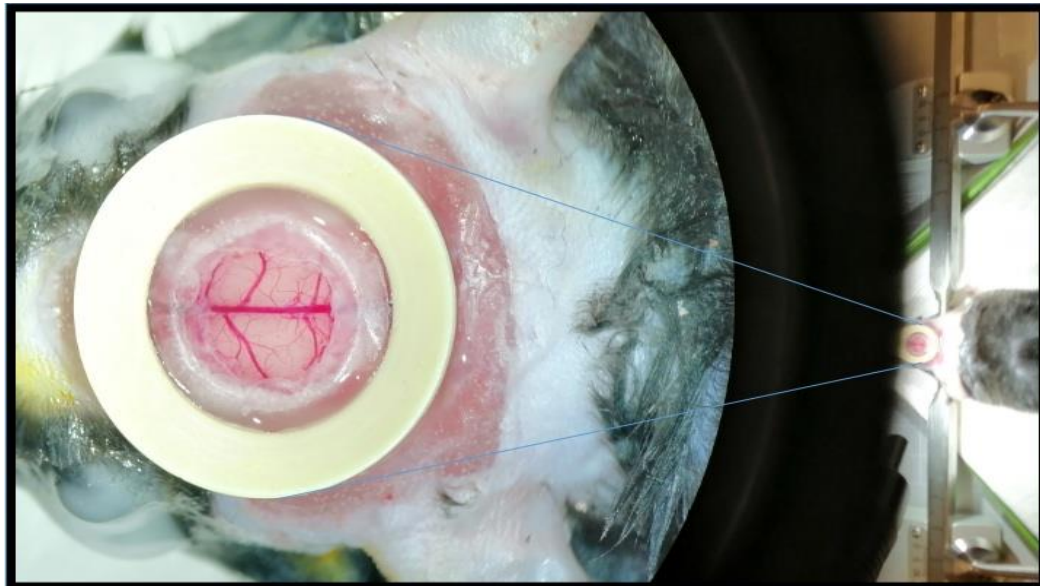


**Figure 8 | Cranial window implantation**

The image shows the OP situs of a mouse was equipped with a cranial glass window and a plastic ring for fixation during in vivo microscopy (left part: view through the OP-microscope eye piece).

---

### 2.10.3 Stereotactic injection of tumor cells and T cells

Stereotactic intracerebral injection of tumor cells was performed 4 weeks after cranial window implantation. To simulate cerebral growth of brain metastases,  $2.5 \times 10^3$  EpCAM-LLC1-tdT cells were resuspended in 1  $\mu$ l PBS and stereotactically injected into the left hemisphere at predefined coordinates (1 mm lateral to the sagittal sinus and 2 mm posterior to the bregma; intraparenchymal depth: 1.5 mm) using a Hamilton gas-tight microinjector (Hamilton, Reno, USA) with a 32 gauge needle (45° bevel degree, Hamilton, Reno, USA). Seven days after tumor cell injection,  $2.0 \times 10^5$  CAR T cells concentrated in 1-2  $\mu$ l PBS were injected 1 mm posterior to the injection point (intraparenchymal depth: 1 mm) as highlighted in Figure 9. Injections of tumor cells and CAR T cells were either done after careful removal of the cover glass (for mice allocated to in vivo imaging or immunohistochemical analysis) or through a burr hole (for mice allocated to survival experiments).

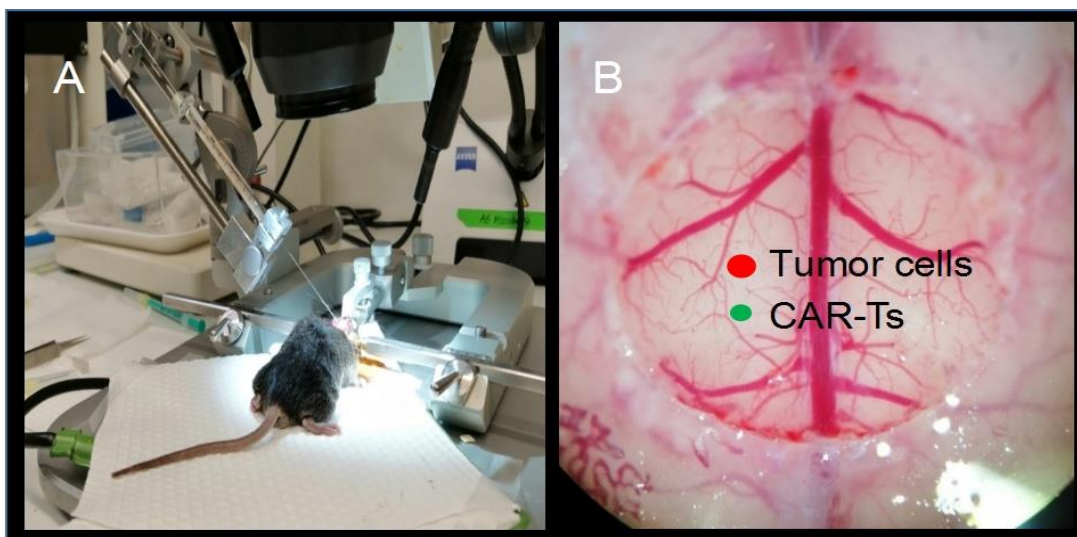


**Figure 9 | Stereotactic injection of tumor cells and CAR T cells**

(A) Stereotactically intracerebral injection of tumor cells was performed 4 weeks after cranial window implantation. After anesthesia and disinfection, mouse was fixed in a stereotactic frame. The CAR or untransduced T cell suspension with a desired concentration was filled

---

into a 10  $\mu$ l Hamilton gas-tight microinjector fixed microsyringe on a stereotactic adapter. (B) shows the injection site of tumor cells and CAR T cells relative to the brain surface and its vascular structure.

### **2.11 In vivo two-photon laser scanning microscopy (TPLSM)**

Metastatic growth was followed by repetitive in vivo microscopy as described previously ([Zhang et al., 2021](#), [Mulazzani et al., 2019](#)). For this purpose, a TrimScope multiphoton microscopy platform (LaVision Biotech TrimScope I) equipped with a MaiTai-laser (wavelength 690-1040nm; Spectra Physics, Newport) and a 4-times objective (numerical aperture: 0.28; XLFluor, Olympus) or a 20-times water immersion objective (numerical aperture: 0.95; XLUMPlanFl, Olympus) was used. Mice were placed on a heating mat during imaging sessions, anesthesia was established with 1% to 2% isoflurane in oxygen adjusted to the breathing rate, and the cranial plastic ring was tightly secured in a custom-made holding device to ensure minimal movements due to breathing. Prior to in vivo microscopy, 100  $\mu$ l fluorescein isothiocyanate (FITC)-dextran (10mg/mL, 2 MDa molecular mass; Sigma-Aldrich) were injected into the tail vein for intravascular plasma staining and, thus, visualization of cerebral blood vessels when appropriate. Recordings were made every 5  $\mu$ m at a wavelength of 920nm, and image resolution was set at  $1024 \times 1024$  pixels. For static analyses, 3D images stack with x/y/z-dimensions of  $450 \times 450 \times 400$   $\mu$ m were acquired and imaging started at the cortical surface (as defined by detection of the arachnoid fibers using second harmonic imaging). For dynamic analyses, 3D images stack with x/y/z-dimensions of  $450 \times 450 \times 66$   $\mu$ m were repetitively acquired over 30 minutes (one recording every 30 seconds) and imaging started 100  $\mu$ m below the cortical surface. Time frame and experimental setup of the

in vivo imaging are highlighted in Figure 10.

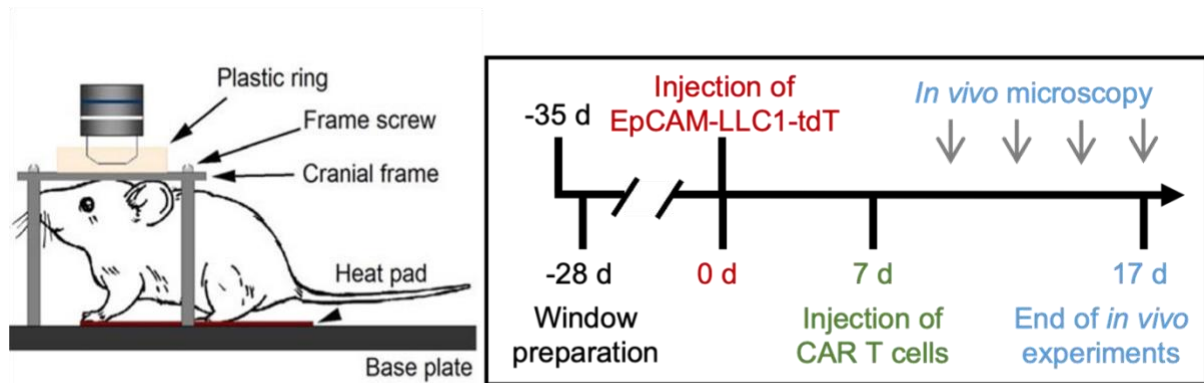


**Figure 10 | In vivo two-photon laser scanning microscopy and the time frame of experiment**

The left part of the schematic shows a mouse with chronic cranial window, fixed on a custom frame through the plastic ring, a 20x water immersion objective was used. During the whole process of imaging, mouse was anesthetized using isoflurane mixed in oxygen at a concentration of 1.0% to 2.0%, and the mouse was kept on a heat pad to keep body temperature stable. The right part of the schematic shows the time frame of experiment. Graphic modified from ([Pérez-Alvarez et al., 2013](#)).

## 2.12 Image analysis

After the raw images from Inspector Pro software (LaVision BioTec) were created, the original images were processed using Imaris software (Bitplane AG, Zurich, Switzerland). Briefly, images were post-processed using the  $3\ \mu\text{m} \times 3\ \mu\text{m} \times 3\ \mu\text{m}$  median filter to remove the background noise. Brightness, contrast, and color balance were manually adjusted to achieve the best image quality. The numbers of CAR T cells expressing GFP were quantified using the spot function of Imaris, while the speed of the T cell movement was measured through the surface function. Mosaic images were generated after 3D image were converted to 2D using the maximum intensity projection (MIP) function. Several MIPs were stitched together to form a big mosaic figure through the MosaicJ function of plugin in ImageJ/Fiji.

---

Epifluorescence microscopy was used to calculate the volume of tumor. Tumor area was assumed according to the maximum 2D diameters (anterior-posterior and left-right) via the following formula:  $\text{area} = \pi \times \text{length}/2 \times \text{width}/2$ .

### **2.13 Statistical analysis**

Statistical analysis was performed using GraphPad Prism software (v9.0). Normal distribution and equal variance of data was tested using the D' Agostino-Pearson omnibus normality-test. Differences were assessed by 2-way ANOVA followed by Sidak's multiple comparisons test, or by the Mann-Whitney U-test (non-parametric data). If not indicated otherwise, all values are expressed as mean  $\pm$  standard error of the mean (SEM). Survival was calculated using Kaplan-Meier survival analysis. The significance level was set at  $p \leq 0.05$ .

---

### 3. Results

#### 3.1 Stable expression of Tdtomato and EpCAM in LLC1

EpCAM-LLC1-tdT cells with strong tdTomato fluorescence and highest EpCAM expression were picked out via repeated FACS sorting. The stability of tdTomato fluorescence and EpCAM epitope expression ratio during 30 days in vitro subculturing was checked regularly using flow cytometry. The intensity of tdTomato fluorescence, with and without the selection antibiotic G418 (Figure 11) as well as the expression of EpCAM (Figure 12) was > 93% over a period of 30 days.

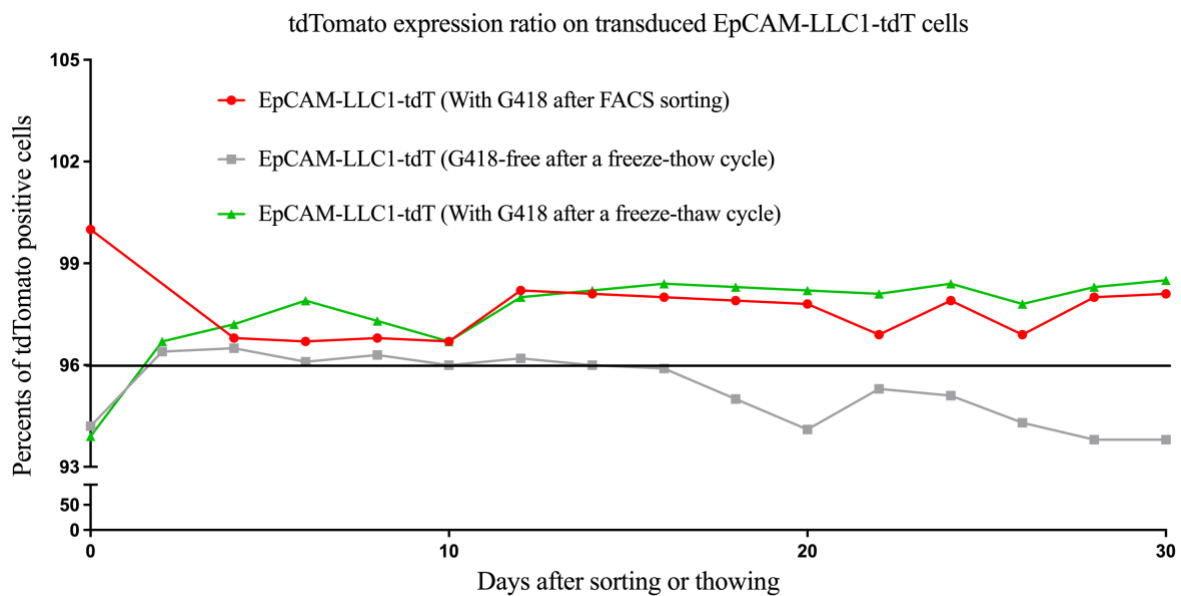


**Figure 11 | For the intensity of tdTomato fluorescence on transduced EpCAM-LLC1-tdT cells**

The red line shows expression ratio of the cells directly subcultured under G418 condition after FACS sorting. Grey line shows cells sub-cultured under G418-free condition after one freeze-thaw cycle. Green line shows cells subcultured under G418 condition after one freeze-thaw cycle. Both of the cells subcultured with G418 highly express tdTomato fluorescence, more than 96% of them are tdTomato positive during 30 days. Even the cells subcultured without G418 have more than 93%.

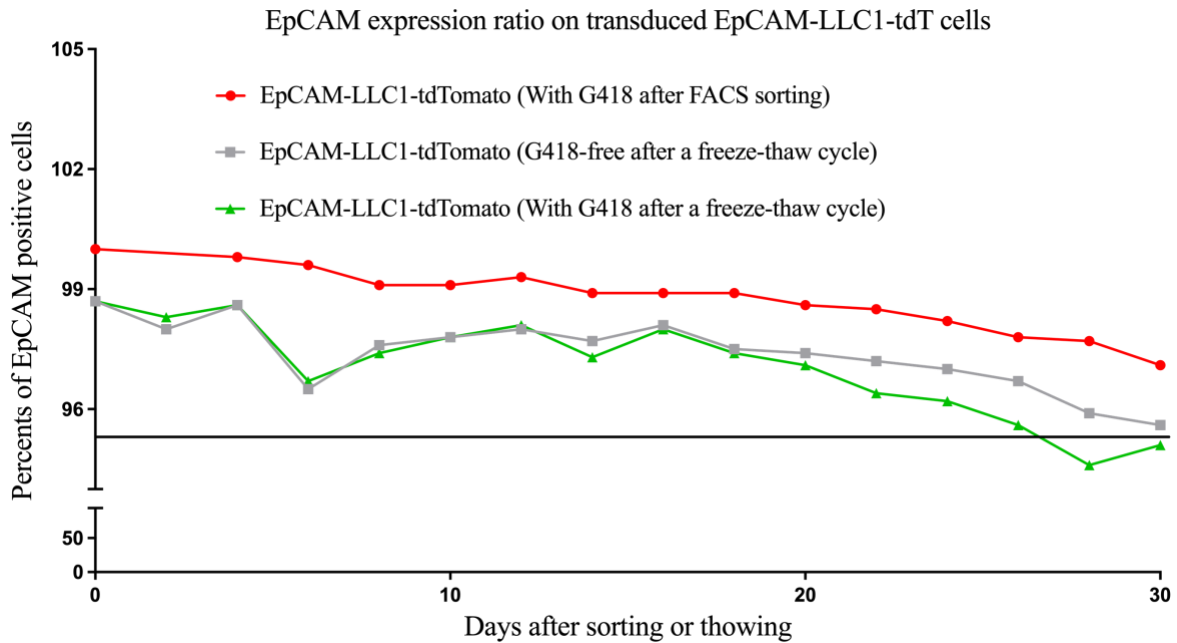


**Figure 12 | For the expression ratio of EpCAM epitope on transduced EpCAM-LLC1-tdT cells**

The red line shows expression ratio of the cells directly subcultured under G418 condition after FACS sorting. The grey line shows cells subcultured under G418-free conditions after one freeze-thaw cycle. Green line shows cells subcultured under G418 condition after one freeze-thaw cycle. Cells expressing EpCAM epitope are more than 95% all three groups during 30 days of subculture.

### 3.2 Establishment of the LCBM animal model

Aseptic inflammation caused by the microsurgical preparation of the cranial window, especially microglia or macrophages activation can impair the growth of lung cancer brain metastasis to some extent. In order to answer the question that how long the activated microglia and macrophages need to recover, transgenic  $CX3CR1^{GFP/WT}$  bearing green fluorescent microglia and macrophages were implanted with chronic cranial window, and imaged regularly (4, 14, 21, 24, 29 days) to assess how long activated microglia or macrophages need to recover after surgery. The morphology of microglia or macrophages was changed. 4 days after cranial window implantation, microglia/macrophages showed signs of

---

activation: the protrusions of microglia/macrophages were shortened, the number of cell protrusions was reduced and the volume of cell body was increased. On day 24 and day 29, obvious cell protrusions were observed, and the cell volume was almost uniform (Figure 13). Therefore, we decided to inject tumor cells 4 weeks after chronic cranial window implantation.

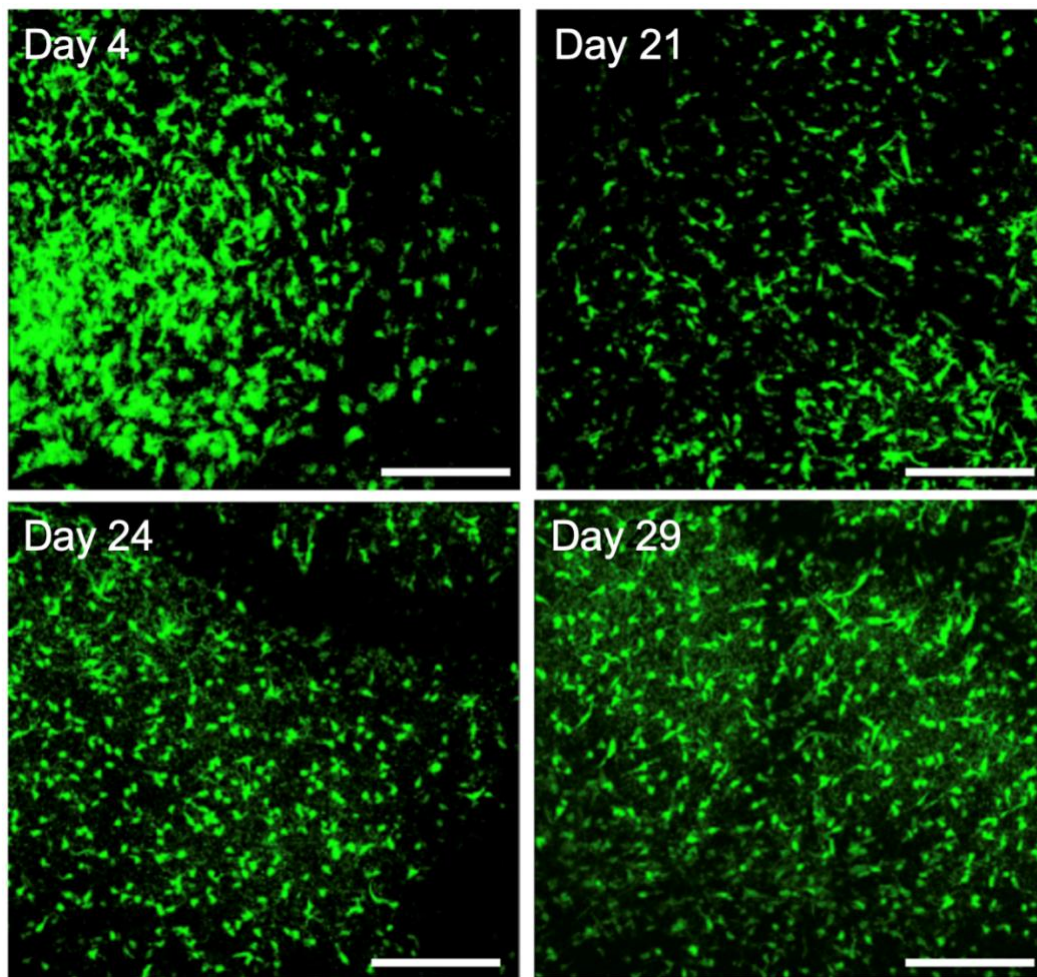


**Figure 13 | The status of microglia/macrophages after cranial window implantation**

The activation of microglia/macrophages caused by the aseptic inflammation after the operation of cranial window implantation. 4 days after cranial window implantation, microglia/macrophages were obviously activated. The protrusions of microglia/macrophages are shortened, the number of cell protrusions is reduced and the volume of cell body is increased. 21 days after cranial window implantation, the protrusions of some cells can be observed, but the volume of the cell body is still uneven. On day 24 and day 29, obvious cell protrusions can be observed, and the cell volume is almost uniform. Maximum intensity

---

projection of a 3D scanning volume (x=450  $\mu\text{m}$ , y=450  $\mu\text{m}$ , z=200  $\mu\text{m}$ ).

### 3.3 Visualization of LCBM growth in vivo

Implantation of a chronic cranial window was well tolerated and allowed for repetitive in vivo imaging using two-photon laser scanning microscopy. After EpCAM-LLC1-tdT cells were intracranially injected into the brain parenchyma, tumor cells were detected based upon their red fluorescence signal. All mice had visible tumor take six days after the tumor cell injection; and rapid growth of solitary lesions was seen in the following days. Fluorescence intensity remained high until the end of the in vivo experiments. Figure 14 shows representative images obtained by in vivo microscopy. 17 days after tumor injection, a large LCBM has formed showing pathologic tumor vascularization.

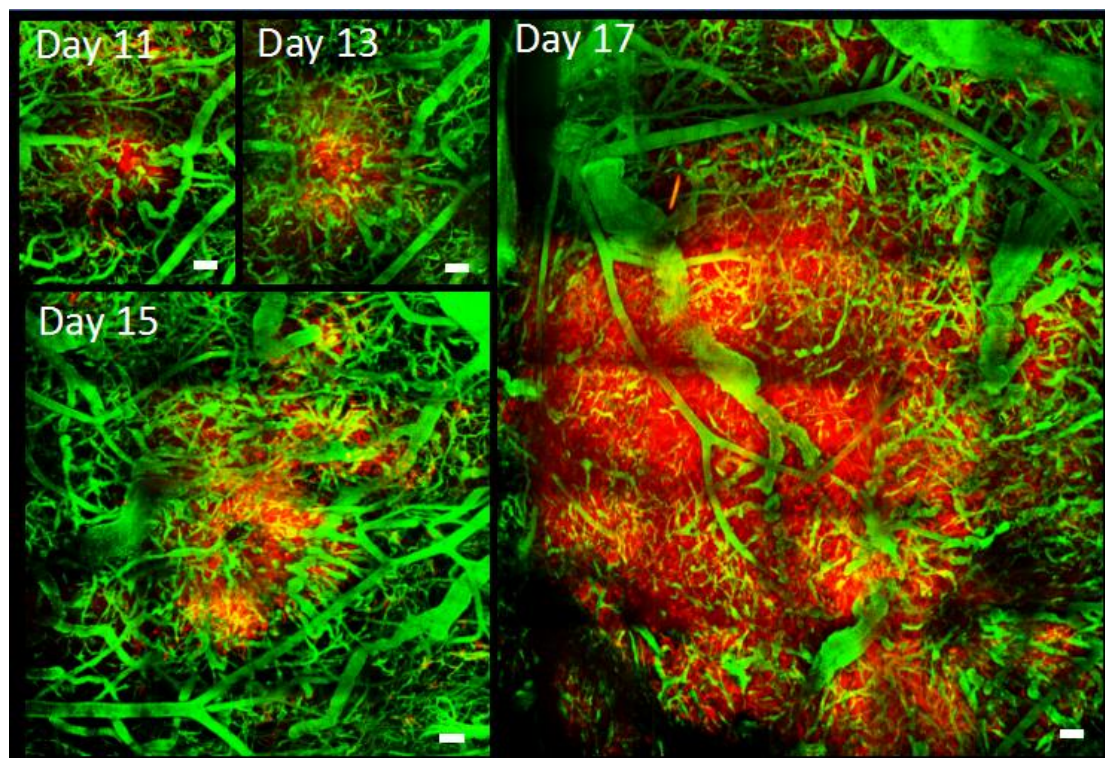


**Figure 14 | Visualization of intracerebral LCBM growth in vivo via two-photon microscopy**

Representative TPLSM images of intracerebral LCBM growth for 17 days after stereotactic

---

intracerebral implantation of  $2.5 \times 10^3$  EpCAM-LLC1-tdT cells. The mosaic figures were created by stitching maximum intensity projections (MIP) with the volume of  $450 \mu\text{m} \times 450 \mu\text{m} \times 400 \mu\text{m}$  (x/y/z) per region of interest (ROI). Blood vessels are highlighted in green after i.v. injection of FITC dextran. Red fluorescent EpCAM-LLC1-tdT cells are displayed in red. Scale bar,  $100 \mu\text{m}$ .

### 3.4 Transduction ratio of CAR T cells

We designed a second-generation murine CAR T cell with a CD28 costimulatory domain targeting EpCAM, which is commonly expressed on lung cancer cells. The GFP sequence is connected to the CAR sequence through P2A. Transduced cells can be sorted and purified by the expression of GFP fluorescent protein (Figure 15).

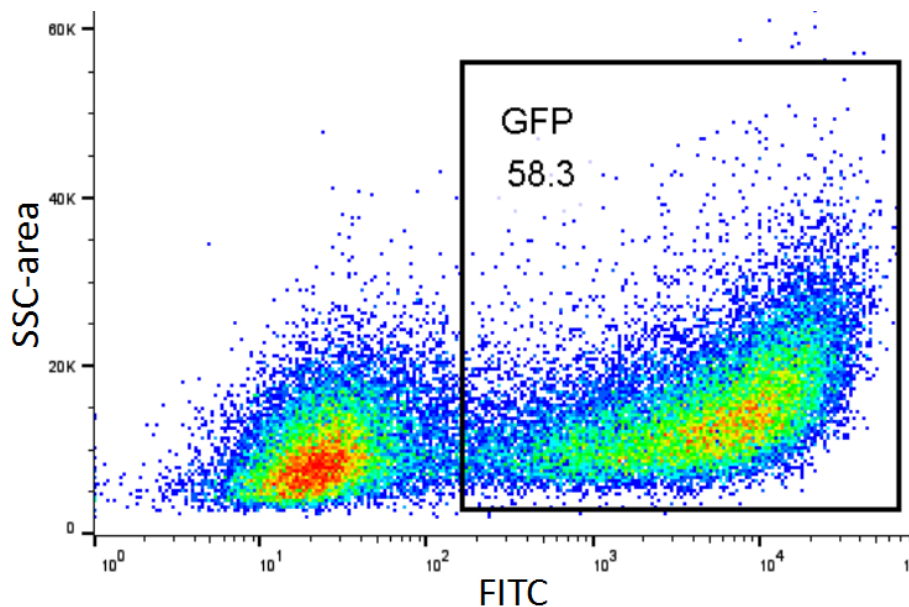


**Figure 15 | Transduction ratio of CAR EpCAM GFP plasmids**

### 3.5 IFN- $\gamma$ release assay

IFN- $\gamma$  is a cytokine that is critical for innate and adaptive immunity. After CAR T cells recognize their specific epitope EpCAM on tumor cells via the CAR, IFN- $\gamma$  is released. The

amount of IFN- $\gamma$  released therefore reflects the ability of specific recognizing tumor antigen and the ability of specific killing tumor. The efficacy of CAR T cells was analyzed in co-culture of CAR T cells or untransduced T cells with EpCAM-LLC1-tdTomato cells or LLC1 cells, and IFN- $\gamma$  in the supernatant was quantified using ELISA. Whereas unidirected T cells did not exert relevant killing activity, the co-culture with CAR T cells resulted in substantial tumor cell lysis translating into increased levels of released IFN- $\gamma$  (Figure 16).

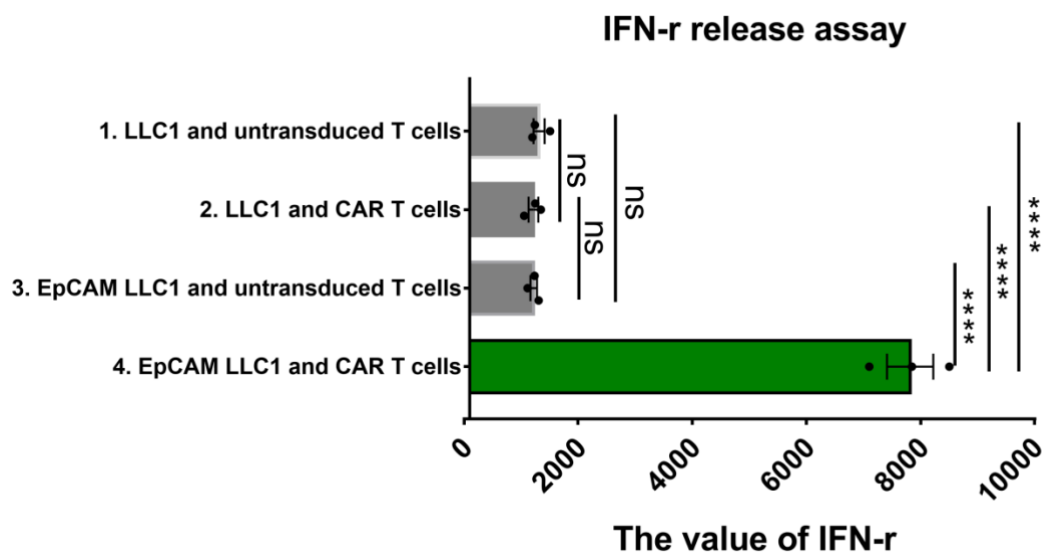


**Figure 16 | In vitro IFN- $\gamma$  release assay**

After 24 hours of co-culture CAR T cells or untransduced T cells with EpCAM-LLC1-tdT cells or LLC1 cells, IFN- $\gamma$  in the supernatant from co-culture medium was measured using ELISA. Whereas untransduced T cells did not exert relevant killing activity, the co-culture with CAR T cells resulted in substantial tumor cell lysis. Mean  $\pm$  S.E.M of triplicate wells. ns = not significant, \*\*\*\*p < 0.0001.

### 3.6 In vivo dynamics of CAR T cells and untransduced T cells after intraparenchymal injection

For in vivo imaging, CAR T Cells or untransduced T cells were injected stereotactically into the mouse cortex 1 mm posterior of the tumor injection site, at a depth of 1 mm 4 days after

---

CAR T cells injection. In vivo microscopy was performed every other day to monitor tumor growth and in vivo dynamics of untransduced T cells and CAR T cells respectively (Figure 17 and Figure 18).

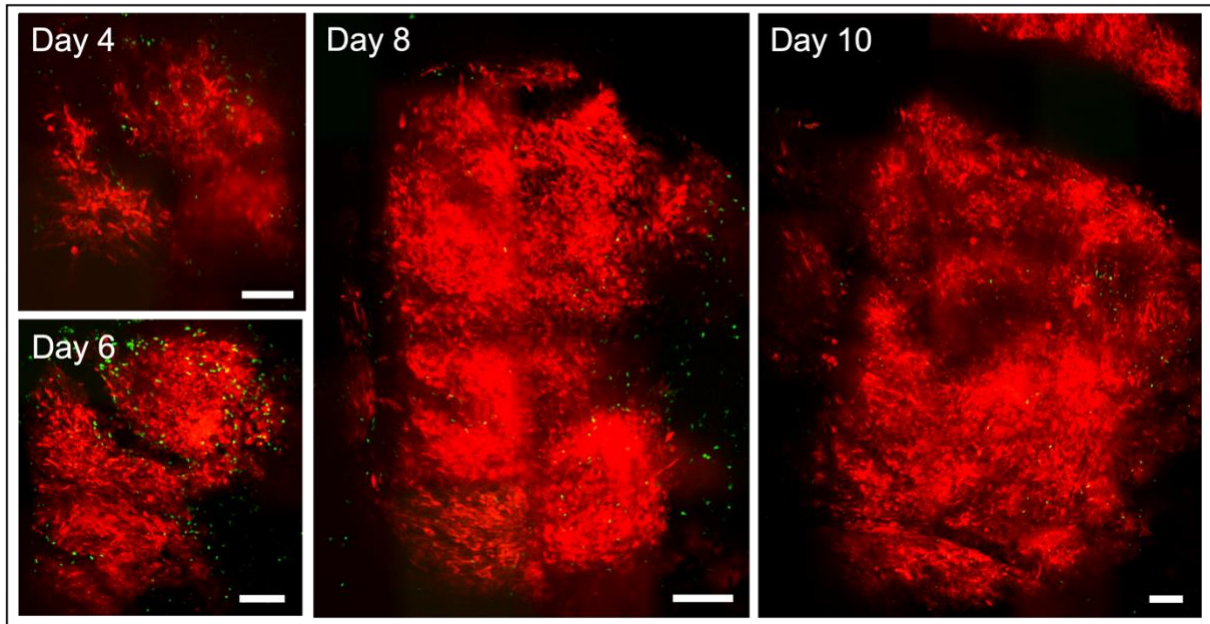


**Figure 17 | In vivo imaging of untransduced T Cells in orthotopic lung cancer brain metastasis**

Representative TPLSM images show different time points after the stereotactic injection of untransduced T cells. The tumor size constantly increased until day 17. The tumor grew in the form of a solid tumor mass, surrounded by satellite lesions of various sizes. Untransduced T cells mainly appeared on the borders of the solid tumors, and the number decreases over time. On day 10 (17 days after tumor cell injection), only a few GFP T cells were visible. The mosaic figures were created by stitching maximum intensity projections (MIP) with the volume of  $450\ \mu\text{m} \times 450\ \mu\text{m} \times 400\ \mu\text{m}$  (x/y/z) per region of interest (ROI). Untransduced T Cells are in green. Tumor cells (EpCAM-LLC-tdT) are in red. Scale bar,  $150\ \mu\text{m}$ .

After injection of untransduced T cells into the cerebral parenchyma adjacent to the tumor, the cells migrated into the brain tumor within days and predominantly accumulated around the tumor borders. The tumor mass constantly expanded over time (Figure 17). In contrast, CAR T cells infiltrated into LCBM more evenly and tumor had an inhibited growth (Figure 18).

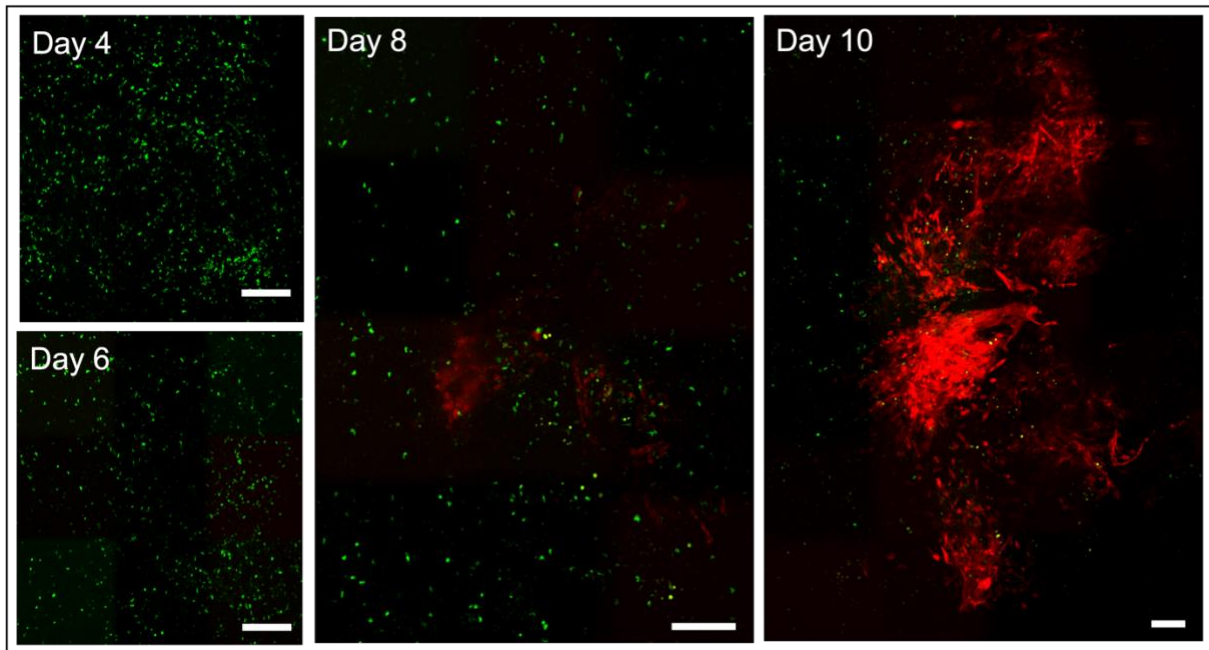


**Figure 18 | In vivo imaging of CAR T cells in orthotopic lung cancer brain metastasis**

Representative TPLSM images show different time points after the stereotactic injection of CAR T cells. On day 4 and day 6, CAR T cells could be detected, however, superficial tumor cells were eradicated. On day 8 and day 10, not only CAR T cells, but also tumor cells from some mouse brains were detectable. Tumors grew slowly. During the observation period of 10 days, CAR T cells decreased. Mosaic figures were created by stitching maximum intensity projections (MIP) with the volume of  $450\ \mu\text{m} \times 450\ \mu\text{m} \times 400\ \mu\text{m}$  (x/y/z) per region of interest (ROI). CAR T Cells are in green. Tumor cells (EpCAM-LLC-tdT) are in red. Scale bar,  $150\ \mu\text{m}$ .

After injection of CAR T cells into the cerebral parenchyma adjacent to the tumor, the cells migrated into the brain tumor within days, which lead to an initial tumor regression. However, the number of CAR T cells decreased over time, which was paralleled by tumor regrowth in some mice (Figure 19).

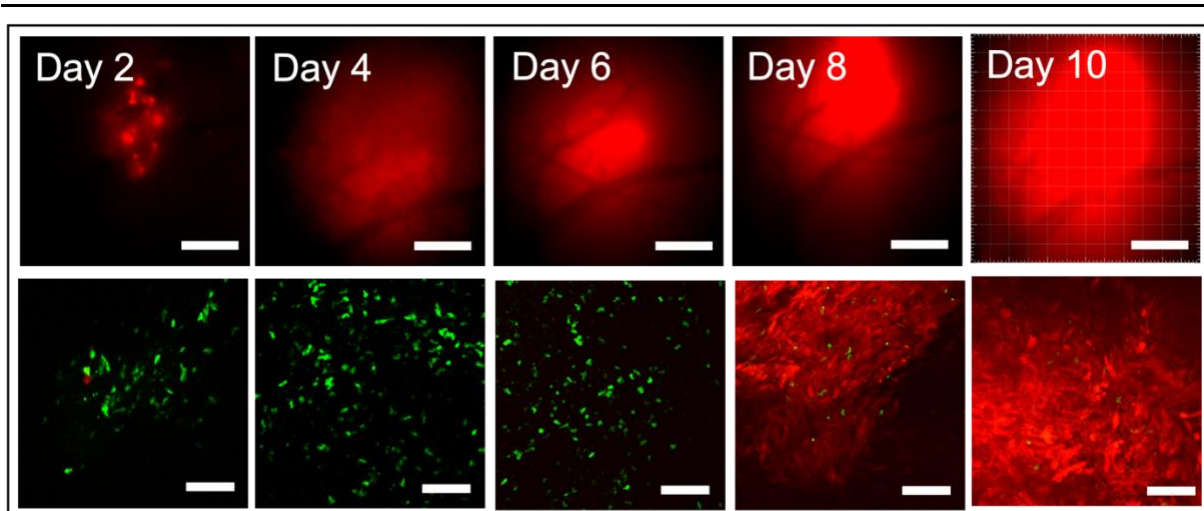


**Figure 19 | In vivo CAR T cell dynamics after intraparenchymal injection and tumor was inhibited**

Representative in vivo images of tumor on days 2, 4, 6, 8, and 10 after intraparenchymal injection of CAR T cells using epifluorescence (upper panel) and two-photon laser scanning microscopy (lower panel). Note the inhibited tumor growth and intratumoral CAR T cell accumulation after administration of CAR T cells. Epifluorescence microscopy images were created by CCD camera in red channel with the area of  $2000\ \mu\text{m} \times 2000\ \mu\text{m}$  (x/y) per region of interest (ROI). Scale bar,  $500\ \mu\text{m}$ . Representative TPLSM images were maximum intensity projections (MIP) with the volume of  $450\ \mu\text{m} \times 450\ \mu\text{m} \times 400\ \mu\text{m}$  (x/y/z) per region of interest (ROI). CAR T Cells are in green. Tumor cells (EpCAM-LLC-tdT) in red. Scale bar of upper panel,  $500\ \mu\text{m}$ . Scale bar of lower panel,  $100\ \mu\text{m}$ .

In 4 out of 10 mice established lung cancer brain metastasis were eradicated. A representative example is highlighted in Figure 20.

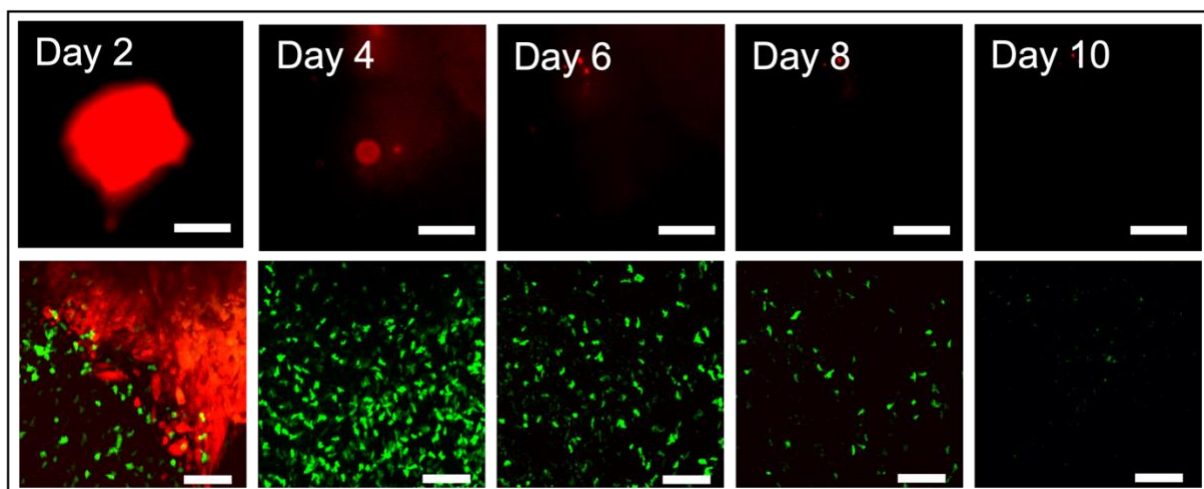


**Figure 20 | In vivo CAR T cell dynamics after intraparenchymal injection and tumor was eradicated**

Representative in vivo images of tumor on days 2, 4, 6, 8, and 10 after intraparenchymal injection of CAR T cells using epifluorescence (upper panel) and two-photon laser scanning microscopy (lower panel). Note the tumor regression and intratumoral CAR T cell accumulation after administration of CAR T cells. Epifluorescent microscopy images were created by CCD camera in red channel with the area of 2000  $\mu\text{m}$  x 2000  $\mu\text{m}$  (x/y) per region of interest (ROI). Scale bar, 500  $\mu\text{m}$ . Representative TPLSM images were maximum intensity projections (MIP) with the volume of 450  $\mu\text{m}$  x 450  $\mu\text{m}$  x 400  $\mu\text{m}$  (x/y/z) per region of interest (ROI). CAR T Cells are in green. Tumor cells (EpCAM-LLC-tdT) are in red. Scale bar of upper panel, 500  $\mu\text{m}$ . Scale bar of lower panel, 100  $\mu\text{m}$ .

In animals receiving untransduced T cells, we found unrestricted tumor growth (Figure 21)

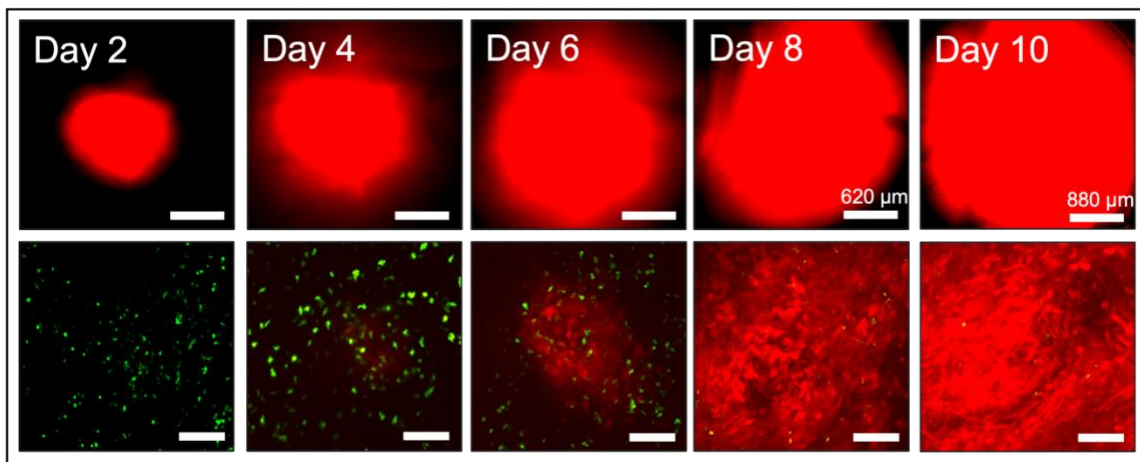


**Figure 21 | In vivo untransduced T cell dynamics after intraparenchymal injection and tumor unrestrictedly grew**

Representative in vivo images of tumor on days 2, 4, 6, 8, and 10 after intraparenchymal injection of untransduced T cells using epifluorescence (upper panel) and two-photon laser scanning microscopy (lower panel). Note the unrestricted tumor growth and reduction of intratumoral untransduced T cell over time. Epifluorescent microscopy images were created by CCD camera in red channel with the area of 2000  $\mu\text{m}$  x 2000  $\mu\text{m}$  (x/y) per region of interest (ROI). Scale bar, 500  $\mu\text{m}$ . Representative TPLSM images were maximum intensity projections (MIP) with the volume of 450  $\mu\text{m}$  x 450  $\mu\text{m}$  x 400  $\mu\text{m}$  (x/y/z) per region of interest (ROI). CAR T Cells are in green. Tumor cells (EpCAM-LLC-tdT) are in red. Scale bar of upper panel, 500  $\mu\text{m}$ . Scale bar of lower panel, 100  $\mu\text{m}$  (except in upper panel, day 8: 620  $\mu\text{m}$  and day 10: 880  $\mu\text{m}$ ).

### 3.7 Anti-tumor cytotoxicity, leading to tumor regression or inhibition

Quantification of tumor growth over time revealed a significant growth delay in animals

---

treated with CAR T cells compared to untransduced T cells (Figure 22). Whereas control mice treated with untransduced T cells showed exponential and rapid tumor growth during the observation period, treatment with CAR T cells resulted in significantly decreased growth (Figure 22).

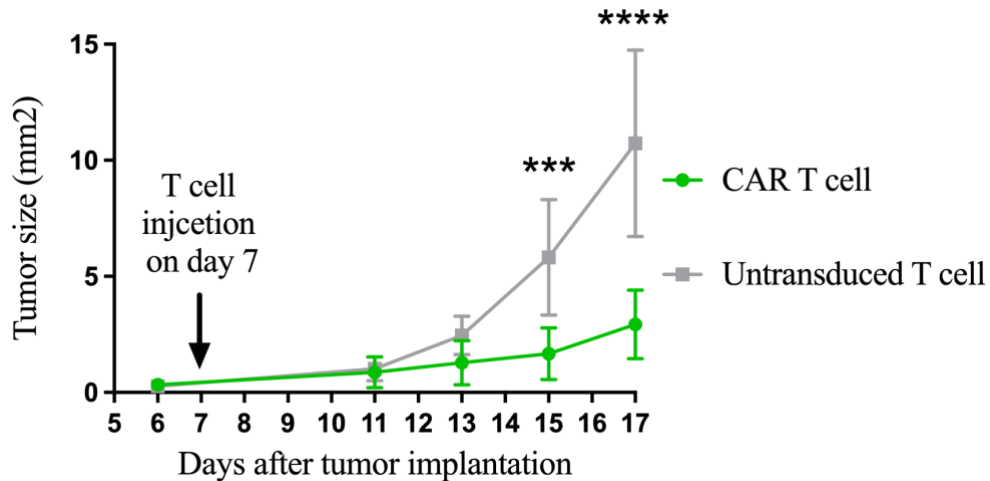


**Figure 22 | Intracranial LCBM growth after injection of CAR T cells**

Tumor volumes of mice receiving CAR T cells (green) or untransduced T cells (grey). Data pooled from independent experiments. Mean  $\pm$  s.e.m. Comparisons were made using 2-way ANOVA followed by Sidak's multiple comparisons test. \*\*\* $p < 0.001$ , \*\*\*\* $p < 0.0001$ ,  $n = 8$  mice (mice receiving untransduced T cells) and 10 mice (mice receiving CAR T cells).

In four out of ten mice (40%) treated with CAR T cells, we even observed complete regression of tumors without any detectable signs of residual lesions at the end of the in vivo microscopy. Moreover, only one animal (10%) which received CAR T cells developed a tumor with  $\geq 5$  mm<sup>2</sup> tumor area, but seven out of eight control mice (87.5%) were found to have large tumors with a 2-dimensional area of  $\geq 5$  mm<sup>2</sup>. After injection of untransduced T cells, 1 of 8 mice (12.5%) showed inhibition of the large, established LCBM, suggesting potential anti-tumor activity of activated T cells (Figure 23).

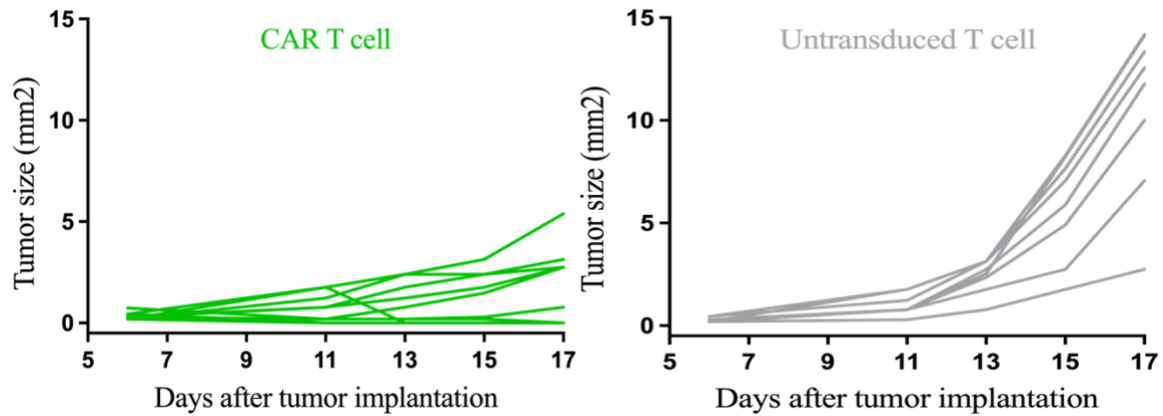


**Figure 23 | Intracranial tumor growth of individual mouse after injection of CAR T cells**

Individual tumor volumes of mice receiving CAR T cells (green) or untransduced T cells (grey). In the untransduced T cell group (n = 8, tumor volume in grey), tumors continuously grow in 8 mice. In 1 of 8 mice, the tumor growth was inhibited. After CAR T cell injection (n = 10, tumor volume in green), tumors in 4 out of 10 mice regressed during the observation period.

### 3.8 The distribution of intratumoral CAR T cells

The ability of T cells to migrate to the tumor area is an important indicator of the ability of T cells to clear tumors. Generally, the stronger the migration ability, the earlier the specific epitopes on the surface of tumor cells can activate CAR T cells, allowing them to exert cytotoxic effects to kill tumor cells, inhibit tumor growth or eliminate tumors. We quantified intratumoral T cell density for CAR T cells and untransduced T cells from 4 to 10 days after stereotactic T cell injection. As expected, on day 4 after T cell injection, both CAR T cells and untransduced T cells were detectable in the tumor area. Intratumoral CAR T cells accumulated in higher numbers compared to untransduced T cells from day 4 to day 8. Especially on the fourth day there was a statistical difference between the two groups. In addition, both CAR T cells in treatment group and untransduced T cells in control group decreased quickly from day 4 to day 10 after treatment (Figure 24).

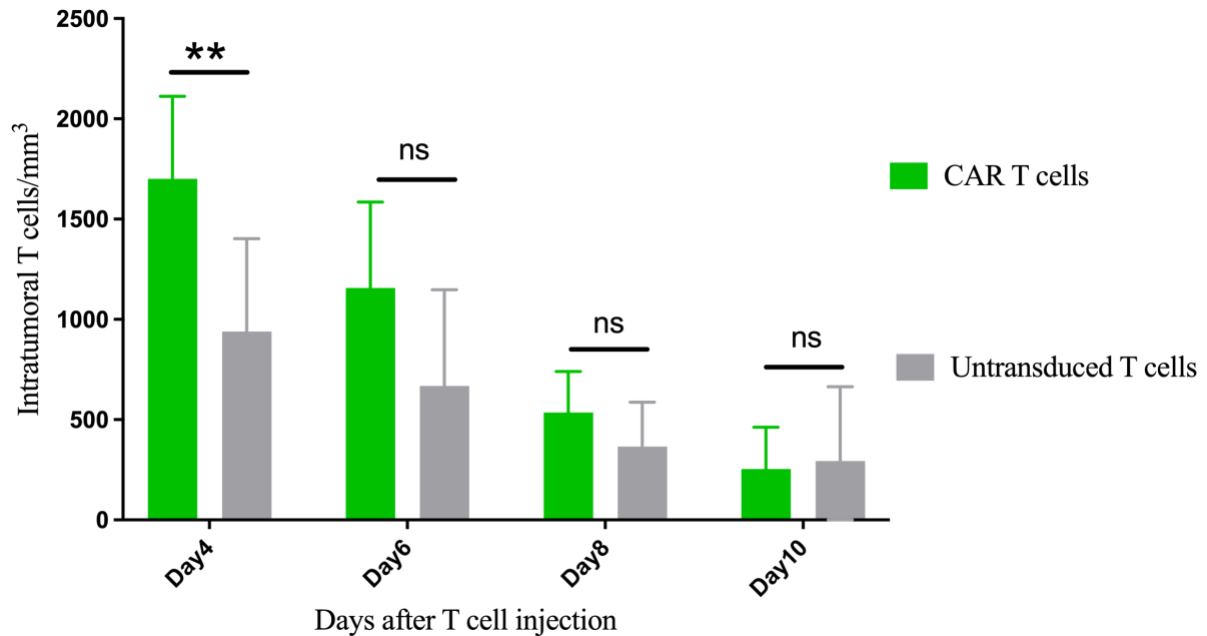


**Figure 24 | Intratumoral CAR T cell or untransduced T cell density**

CAR T cells show higher intratumoral numbers, compared to untransduced T cells from day 4 to day 8. The number of CAR T cells and untransduced T cells reaches their peak value on the fourth day, however, both CAR T cells in treatment group and untransduced T cells in control group were decreased quickly from day 4 to 10 after treatment. T cell numbers quantified of 1 to 2 three-dimensional ROIs from 7 mice per group per time point. Pooled data from 6 independent experiments. Mean  $\pm$  s.e.m. Comparisons were made using 2-way ANOVA followed by Sidak's multiple comparisons test.  $**p < 0.01$ .

We quantified the intratumoral CAR T cell density on the tumor injection site and on the contralateral hemisphere. As expected, CAR T cells were found in both at the tumor injection site and the contralateral tumor injection site from the fourth day to the tenth day after treatment. The number of Intratumoral CAR T cells on the tumor implantation side was higher than that in the contralateral brain hemisphere, especially on the fourth and sixth days, the number of CAR T cells on the tumor implantation side was significantly higher than that in the contralateral brain hemisphere. Apparently, CAR T cells are mainly recruited to the tumor implantation site, however, may also play an immune surveillance function in the

contralateral brain hemisphere (Figure 25).

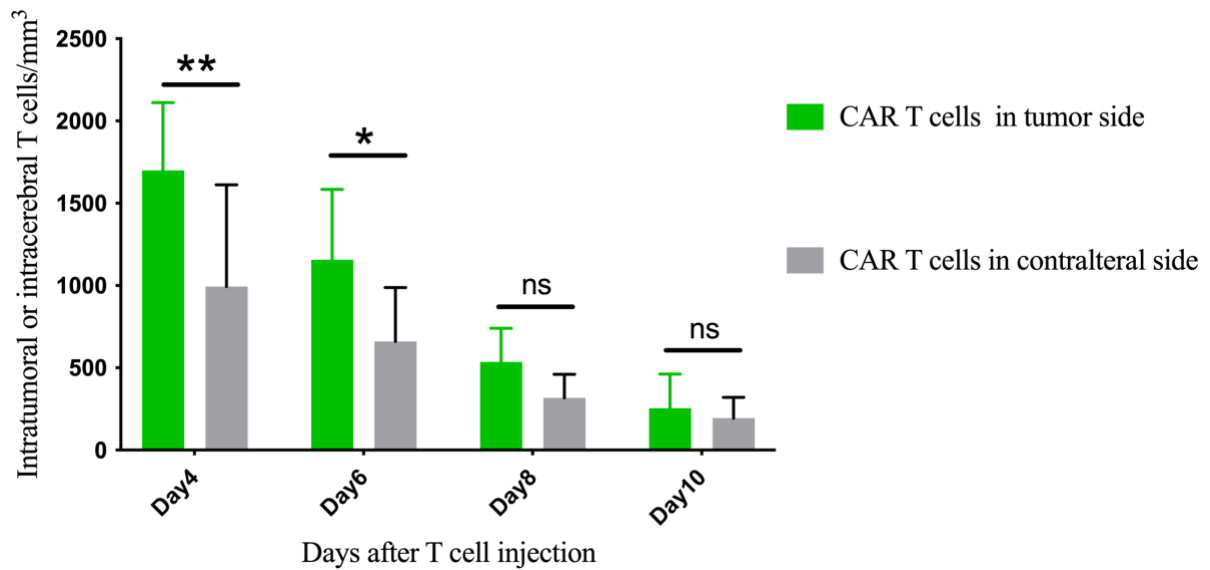


**Figure 25 | Intratumoral and contralateral CAR T cell density**

CAR T cells show higher intratumoral numbers at tumor implantation site, compared to the contralateral hemisphere at all time points after treatment. CAR T cells number quantified of 1 to 2 three-dimensional ROIs from 7 mice per group per time point. Pooled data from 6 independent experiments. Mean  $\pm$  s.e.m. Comparisons were made using 2-way ANOVA followed by Sidak's multiple comparisons test. \* $p < 0.05$ , \*\* $p < 0.01$ .

In the control group, untransduced T cells were found in the tumor injection site and in the contralateral hemisphere from the fourth day to the tenth day after treatment. The number of intratumoral untransduced T cells was not significantly different to the contralateral hemisphere (Figure 26).

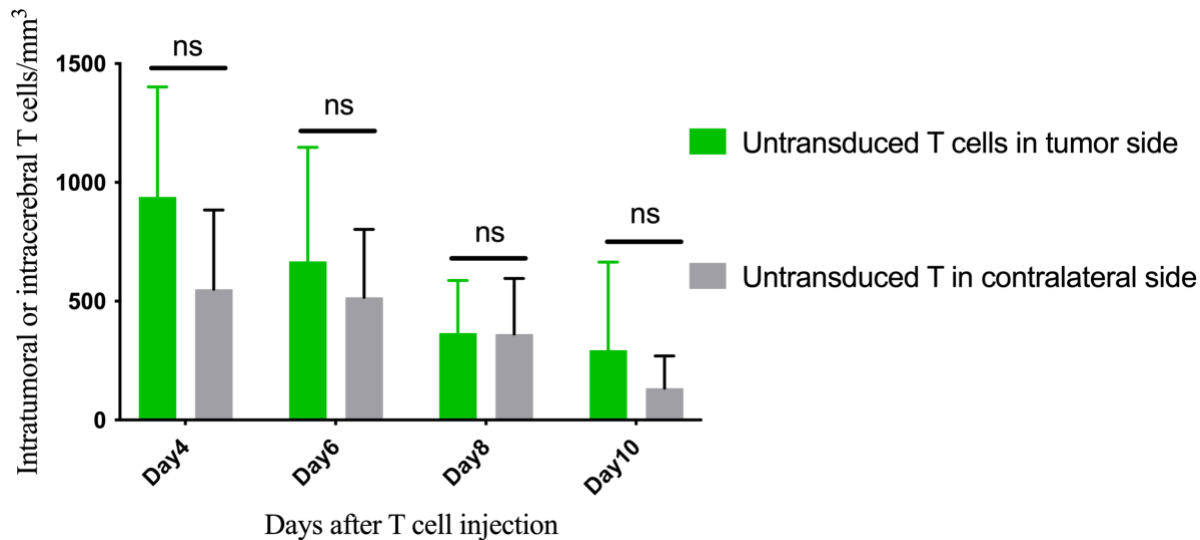


**Figure 26 | Intratumoral and contralateral untransduced T cell density**

Untransduced T cells were found in both of the tumor implantation site and contralateral to the tumor implantation site all time points after treatment with no significant difference in distribution. Untransduced T cell numbers were quantified in 1 to 2 three-dimensional ROIs from 7 mice per group per time point. Pooled data from 6 independent experiments. Mean  $\pm$  s.e.m. Comparisons were made using 2-way ANOVA followed by Sidak's multiple comparisons test. ns = not significant.

### 3.9 The velocity of Intratumoral CAR T cells

TPLSM can not only capture the number of CAR T cells in the tumor and their distribution, but can also be used to visualize the behavior of individual T cells over time by making 3D time-lapse movies. We therefore measured the difference of velocity between untransduced T cell migration and CAR T cell migration during tumor growth and regression. On day 4 after T cell i.c. injection, we found no significant difference of velocity between CAR T cells and untransduced T cells. However, on day 8 after T cell i.c. injection, intratumoral CAR T cell velocity was slower than mock CAR T cell velocity (Figure 27). T cell receptor (TCR)-mediated anti-tumor cytotoxicity has been characterized by long-lasting contacts between effector immune cells and tumor cells ([Breart et al., 2008](#)), which may explain the

reduced velocities.

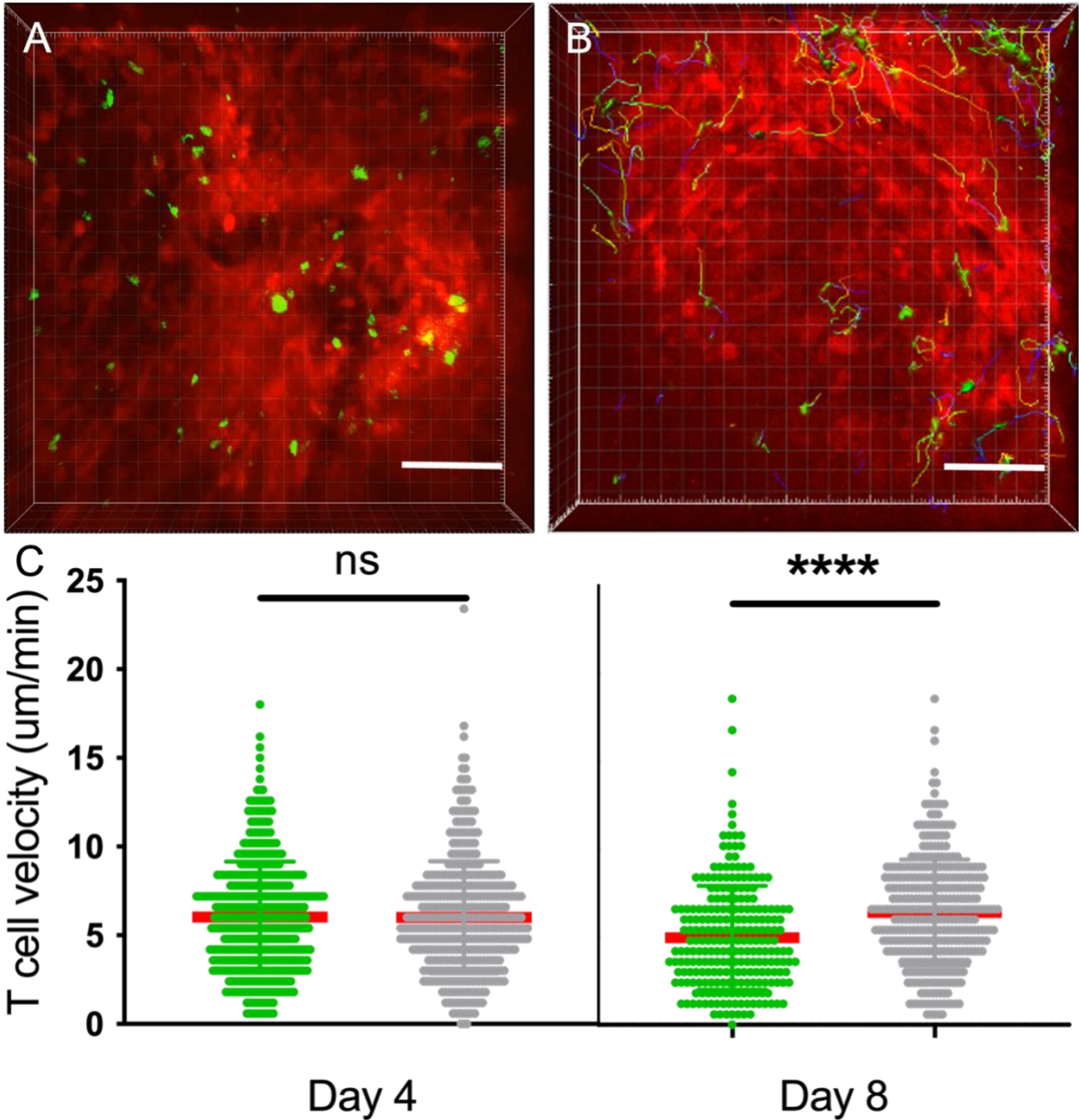


**Figure 27 | Intratumoral CAR T cell and untransduced T cell velocity**

Examples of (A) TPLSM images of EpCAM-LLC-tdT cells (red), CAR T cells (green) and (B) three-dimensional reconstruction of untransduced T (green) with intratumoral migration tracks. Time lapse movie of 30 minutes duration, 8 days after i.c. injection. C) Quantification of individual, intratumoral T cell velocity of migration tracks as shown in (B). Each green dot represents one CAR T cell. Results from pooled time lapse microscopy movies of at least 30 minutes duration (recording every 30 seconds) per time point, ROI of 450  $\mu\text{m}$  x 450  $\mu\text{m}$  x 66  $\mu\text{m}$  (x/y/z) starting at least 100  $\mu\text{m}$  underneath the brain surface. There was no significant difference of velocity between CAR T cells and untransduced T cells on day 4 after treatment. However, intratumoral CAR T cell velocity was slower than untransduced T cell velocity on day 8 after i.c. injection. Pooled data from 6 independent experiments. Median +/-

interquartile range. Comparisons were made using the Mann-Whitney U test. ns = not significant, \*\*\*\* $p < 0.0001$ .

### 3.10 Blood sampling

In order to assess whether CAR T cells enter the blood circulation, potentially resulting in off-target effects at remote sites, we assessed their presence in the peripheral blood using flow cytometry. Both on day 4 and day 10 after stereotactic T cell i.c. injection, CAR T cells and untransduced T cells were not detected in the peripheral circulation. There was no significant difference between CAR T cell treated mice and untreated mice (Figure 28, right), or untransduced T cell treated mice and untreated mice (Figure 28, left).

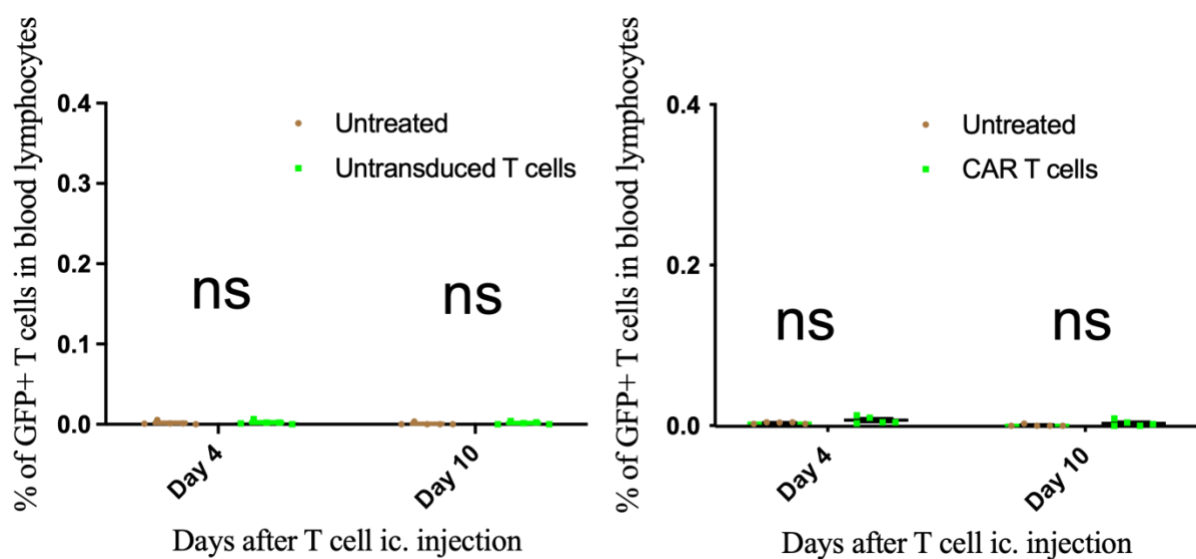


**Figure 28 | Flow cytometry of CAR T cells and untransduced T cells in the peripheral blood**

Both on day 4 and day 10 after i.c. injection, CAR T cells and untransduced T cells were almost undetectable in the peripheral blood. The graph displays the fraction of CAR T cell (right) or untransduced T cell (left) of all lymphocytes in blood measured by FACS analysis. Untreated mice (grey;  $n = 5$ ), untransduced T cells (green;  $n = 5$ ), and CAR T cells (green;  $n = 5$ ). Results from 2 independent experiments. Comparison was made using 2-way ANOVA followed by Sidak's multiple comparisons test. ns = not significant.

---

### 3.11 Survival rates

We used C57BL6J mice receiving tumor cell and CAR T injections via a bur hole for survival analysis experiments. We found that the survival time of animals receiving CAR T cells was longer than that of the control group, and the difference was statistically significant. We found a median survival was prolonged in mice in which CAR T cells were provided (CAR T cells: 22 days versus untransduced T cells: 20 days). One mouse in CAR T cell group live more than 83 days indicating potential cure (Figure 29).

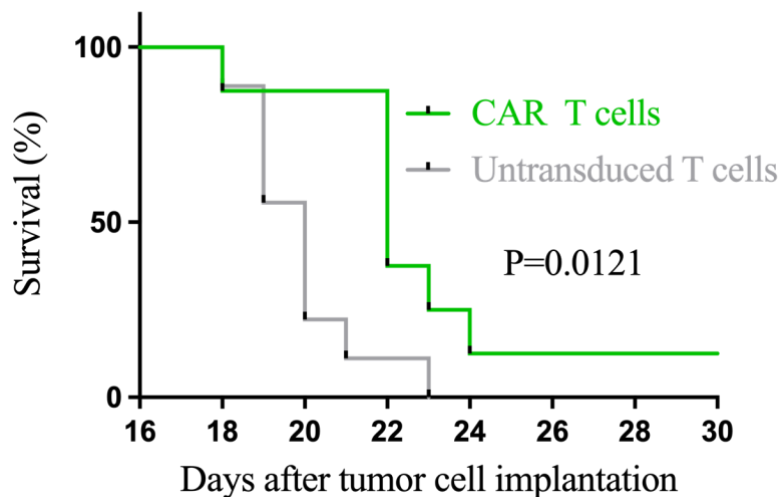


**Figure 29 | Survival rates after CAR T cells or untransduced T cells i.c. injection**

The graph highlights the survival after treatment with CAR T cells (green line, n=8) or untransduced T cells (grey line, n=9). Mice in CAR T cell group have longer survival time than mice in untransduced T cell group. One mouse in CAR T cell group live more than 83 days. Data pooled from 4 independent experiments. Comparison of survival rates was performed with the Kaplan-Meier estimate.

---

## 4. Discussion

Lung cancer patients with brain metastases identify with a devastating natural history, and innovative therapeutic approaches are urgently needed for this patients population ([Shaw et al., 2020](#), [Lee and Ahn, 2021](#)). In this doctoral these repetitive in vivo imaging through a cranial window was combined with intraparenchymal injections of fluorescent lung cancer cells and CAR T cells which offered the exciting opportunity to assess the real time properties of CAR T cells in the brain on a single cell level. Based on this fully immunocompetent model, the promising anti-tumor properties of CAR T cells for brain metastases from lung cancer could be illustrated.

### 4.1 Mouse model

In this study, a syngeneic orthotopic mouse model was developed to study LCBM. Repeated TPLSM through a chronic cranial window enabled analyzing LCBM growth in unprecedented detail. It is known, that the therapeutic efficacy of CAR T highly depends on their migration towards and recruitment into brain tumors, as well as their activity and persistence in the immunosuppressive tumor microenvironment ([Shiina et al., 2016](#), [Weiss et al., 2018](#), [Haydar et al., 2021](#)). However, so far our group was the first to be able to analyze these processes at the single cell resolution level and to track the kinetic characteristics of intracerebral CAR T cells in the same animal repeatedly by combining chronic cranial windows with TPLSM ([Mulazzani et al., 2019](#)). Unlike in this previous study, in this thesis a syngeneic model was developed. This is very important as the use of human cancer cells in immunodeficient mice

---

does not reflect the immunosuppressive effect of e.g. regulatory T cells (Treg) ([Maj et al., 2017](#), [Bull et al., 2018](#), [Son et al., 2020](#)). However, the animal models have some limitations. For this study male C57Bl6j mice were used as recipients and allogeneic male C57Bl6j mice were used as T cell donors. Compared with using xenograft mouse model, the recipient mice in this study have greater immune rejection for implanted T cells, which makes the therapeutic effect of CAR T cells to a certain extent underestimated. Compared with clinical patients who use autologous T cells for genetic modification and amplification in vitro and then infused into the patient's body, the effect of CAR T cell therapy in this study may be further underestimated. Brain metastases from lung cancer in mice grow rapidly ([Hsu et al., 2019](#), [Masuda et al., 2020](#), [Zhang et al., 2021](#)). In our study, CAR T cells were used on the seventh day after intracranial tumor cell implantation. In the first three days after intracranial injection of CAR T cells, an image with high quality cannot be obtained due to aseptic inflammation inside the cranial window. Therefore, quantification of CAR T cells starts on the fourth day (equivalent to the 11th day after tumor implantation) until the end of the experiment (equivalent to 17th day after tumor implantation), the time window of two-photon microscopy is only 7 days. Some very interesting phenomena may be outside this time window.

#### **4.2 CAR T cells treatment**

We found that treatment with CAR T cells injected into the cerebral parenchyma did not only result in decreased growth of lung cancer brain metastasis but also in complete tumor

---

regression in some mice. These anti-tumor effects indeed translated into a considerable survival benefit of mice treated with CAR T cells including long-lasting remission. Encouraging findings have been made in preclinical *in vivo* models assessing intracranially administered CAR T cells for the treatment of primary CNS malignancies including CNS lymphoma ([Mulazzani et al., 2019](#)), medulloblastoma ([Donovan et al., 2020](#)), or glioblastoma ([Wang et al., 2020](#)); as well as for secondary CNS malignancies such as breast cancer metastases ([Priceman et al., 2018](#)). Although such favorable results have encouraged ongoing clinical CAR T cell trials for brain tumor patients ([Karschnia et al., 2021](#)), none of these studies yet includes lung cancer patients. Our present study appears to support that CAR T cell therapy might also warrant evaluation in individuals with brain metastases from lung cancer.

#### **4.3 Recruitment of CAR T cells into solid tumor**

An important step for successful CAR T treatment is tumor infiltration. In solid tumors, CAR T cells have to overcome a variety of physical and immune barriers ([Rafiq et al., 2020](#), [Johnson et al., 2021](#)). Until now, only very few studies have reported the visualization of CAR T cells entering solid tumors and the dynamic changes between tumor cells and CAR T cells in mouse orthotopic tumor models ([Mulazzani et al., 2019](#)).

Our model allowed to dissect the *in vivo* dynamics of CAR T cells, and our analysis at early days after CAR T cell injection showed a higher density of intratumoral CAR T cells which were more evenly distributed throughout the tumor compared to undirected T cells serving as

---

controls. This observation indicates enhanced proliferation, migration, and tumor infiltration of directed CAR T cells. Although the exact mechanisms remain elusive, early antigen contact of the CAR T cells with the EpCAM-expressing tumor cells might have contributed to these effects. Such an interaction substantially stimulates differentiation, proliferation, and survival of T cells ([Kaech and Ahmed, 2001](#), [Shyer et al., 2020](#)).

#### **4.4 The persistence of CAR T cells**

The number of CAR T cells declined rapidly, pointing towards insufficient persistence of CAR T cell within the tumor tissue. The CAR T cell density within the tumor was comparable to controls at the end of the *in vivo* experiments, and this was often paralleled by tumor growth. These findings seem consistent with preclinical and clinical reports of rapidly decreasing CAR T cell numbers in solid brain tumors as glioma ([Brown et al., 2015](#)).

Clinical trials for brain tumor patients evaluating concepts to counteract the insufficient persistence by stimulation of CAR T cells with immunotherapies such as checkpoint inhibitors are ongoing (NCT04003649) ([Blaeschke et al., 2021](#)). In this context, CAR T cells entering the systemic circulating (and homing into nondraining lymph nodes) following intracranial injection have been identified as a reservoir protecting against local tumor recurrence in the CNS ([Mulazzani et al., 2019](#), [Wang et al., 2021](#)). However, in this study, the CAR T cells in peripheral taking blood samples was almost undetectable, and it appears therefore unlikely that such a blood infiltration might have taken place in our study. If administered, the use of lymphodepletion prior to CAR T cell administration could have

---

increased the systemic quantity and persistence of CAR T cells ([Sampson et al., 2014](#)).

A possible strategy to enhance the CAR T tropism to brain tumors is to express chemokine receptors that match to chemokines that are expressed in the respective tumor ([Lesch et al., 2021](#)). In addition, other studies have also shown that chemokine receptors may be one way to improve T cell trafficking, and then increase T cell persistence, thereby increasing anti-tumor efficacy ([Jin et al., 2019](#), [Cadilha et al., 2021](#)).

#### **4.5 Intratumoral CAR T cells velocity**

TPLSM can describe the interaction between CAR T cells and cancer cells in the process of tumor growth or regression at the single-cell resolution level. For example, our group has shown that CAR T cells directed against CD19 are able to infiltrate intracranial lymphoma in high numbers, leading to elimination of this CD19 expressing, solid tumor ([Mulazzani et al., 2019](#)). In this study, the velocity of mock CAR T cell and h19m28z CAR T cell was compared. Interestingly, during the early stages of tumor cell killing, infiltrating h19m28z CAR T cells have a lower intratumoral velocity, and kill tumor cells. Conversely, mock CAR T cells which cannot specifically recognize CD19 expressing lymphoma cells have a higher migratory velocity inside the tumor, and neither kill lymphoma cells and nor stop their own movement. It suggested that lower intratumoral velocity is associated with CAR-mediated tumor cell killing. Cadilha and colleagues found an enhanced infiltrative capacity of CCR8-transduced T cells compared to untransduced T cells in tumor tissue through intravital microscopy. However, no significant changes in the speed of CCR8-transduced T cells inside the tumor

---

compared to untransduced T cells ([Cadilha et al., 2021](#)). From the side, it is possible that the CAR-mediated tumor killing process is one of the reasons for the slowing down of CAR T cell motility.

In our study, we measured the velocity of untransduced T cell and CAR T cell migration on the fourth and eighth days after CAR T cells i.c. injection. The CAR T cells show a similar velocity as untransduced T cells on day 4 after T cell i.c. injection. The possible reason is on the fourth day after the mouse LCBM received CAR T cell treatment, the tumor regressed within the observable range of two-photon microscope, and the CAR T cell movement speed was less affected by the EpCAM antigen. However, CAR T cell migratory velocity was slower than untransduced T cells on day 8 after T cell i.c. injection. The possible reason is the number of T cells declined rapidly 8 days after CAR T cell injection, while tumor cells grew rapidly. So the motility of CAR T cell inside the LCBM of the observable range of two-photon microscope is significantly affected by EpCAM antigen. Therefore, the result of the CAR T cell migratory velocity in this study is consistent with the results of Mulazzani and colleagues.

#### **4.6 Limitations**

We herein performed repetitive in vivo imaging through a cranial window to monitor lung cancer brain metastasis growth after intracranial CAR T cells injection, which offered the exciting opportunity to assess real time dynamics of CAR T cells in the brain at a single-cell level. However, in this study, we only observed the depth within 400  $\mu\text{m}$  from brain surface.

---

The deeper part could not be imaged, and the dynamic characteristics of immune cells and tumor cells could not be further analyzed as well. Given the cranial window implantation for mice produce strong aseptic inflammation (Figure 13), the activation of immune cells, including microglia or macrophages, may not only affect the growth of tumor cells, but also increase the scattering phenomenon during the imaging process and then reduce the quality of the image. In order to get optimal images, tumor cells were injected 4 weeks after cranial window implantation. Since we used a fully immune-competent syngeneic orthotopic mouse model, the persistence of CAR T cells in this study is limited after implantation into mouse brains, the number has been significantly reduced over time.

#### **4.7 Clinical relevance**

We made use of CAR T cells injected into the cerebral parenchyma adjacent to the brain tumor. Whereas we and others observed promising anti-tumor effects using this approach ([Brown et al., 2015](#), [Wang et al., 2021](#)), systemic routes of administration (including intravenous or intraperitoneal injection) have shown less encouraging results in CNS disease ([Mulazzani et al., 2019](#), [Wang et al., 2021](#), [Agliardi et al., 2021](#)). Whether similar observations would also have been made in our model remains speculative; however, based on previous reports it appears highly unlikely that more efficient anti-tumor effects would have been noted after systemic administration of CAR T cells. It remains to be noted that brain metastases are often disseminated within the cerebral parenchyma, and systemic routes might be particularly beneficial in controlling or preventing micrometastatic disease.

---

Brain metastases from lung cancer are particularly prone to create an immunosuppressive niche composed of neoplastic as well as non-neoplastic cells including tumor-associated macrophages and microglia ([Zhang et al., 2021](#)). It remains to be seen whether the immunosuppressive microenvironment of brain metastases from lung cancer may represent an interesting target to further increase the efficiency of CAR T cell based immunotherapy ([Karschnia et al., 2021](#), [Cadilha et al., 2021](#)). Given that our preclinical findings were made in a fully immunocompetent murine model, our encouraging results may have particularly substantial translational implications.

---

## 5. Conclusion

Collectively, the present study highlights the encouraging anti-tumor effects of intracranially injected CAR T cells against solid brain metastases from lung cancer. Migration towards the tumor as well as intratumoral CAR T cells accumulation were associated with tumor regression early after the intraparenchymal injection; however, decreasing CAR T cell numbers during the late observation period suggest insufficient persistence which might be paralleled by tumor regrowth. Given the complex interaction of CAR T cells with the immunosuppressive tumor microenvironment of brain metastases, improved CAR design and the choice of concurrent therapies may further boost the success of CAR T cell therapy for brain metastases. The herein introduced murine model might be a useful tool to evaluate such approaches.

---

## 6. References

- AGLIARDI, G., LIUZZI, A. R., HOTBLACK, A., DE FEO, D., NÚÑEZ, N., STOWE, C. L., FRIEBEL, E., NANNINI, F., RINDLISBACHER, L., ROBERTS, T. A., RAMASAWMY, R., WILLIAMS, I. P., SIOW, B. M., LYTHGOE, M. F., KALBER, T. L., QUEZADA, S. A., PULE, M. A., TUGUES, S., STRAATHOF, K. & BECHER, B. 2021. Intratumoral IL-12 delivery empowers CAR-T cell immunotherapy in a pre-clinical model of glioblastoma. *Nat Commun*, 12, 444.
- BACHANOVA, V., BISHOP, M. R., DAHI, P., DHOLARIA, B., GRUPP, S. A., HAYES-LATTIN, B., JANAKIRAM, M., MAZIARZ, R. T., MCGUIRK, J. P., NASTOUPIL, L. J., OLUWOLE, O. O., PERALES, M. A., PORTER, D. L., RIEDELL, P. A. & CONSORTIUM, C. T. C. 2020. Chimeric Antigen Receptor T Cell Therapy During the COVID-19 Pandemic. *Biol Blood Marrow Transplant*, 26, 1239-1246.
- BENMEBAREK, M. R., KARCHES, C. H., CADILHA, B. L., LESCH, S., ENDRES, S. & KOBOLD, S. 2019. Killing Mechanisms of Chimeric Antigen Receptor (CAR) T Cells. *Int J Mol Sci*, 20.
- BLAESCHKE, F., STENGER, D., APFELBECK, A., CADILHA, B. L., BENMEBAREK, M. R., MAHDAWI, J., ORTNER, E., LEPENIES, M., HABJAN, N., RATAJ, F., WILLIER, S., KAEUFERLE, T., MAJZNER, R. G., BUSCH, D. H., KOBOLD, S. & FEUCHTINGER, T. 2021. Augmenting anti-CD19 and anti-CD22 CAR T-cell function using PD-1-CD28 checkpoint fusion proteins. *Blood Cancer J*, 11, 108.
- BOIRE, A., BRASTIANOS, P. K., GARZIA, L. & VALIENTE, M. 2020. Brain metastasis. *Nat Rev Cancer*, 20, 4-11.
- BRAY, F., FERLAY, J., SOERJOMATARAM, I., SIEGEL, R. L., TORRE, L. A. & JEMAL, A. 2018. Global cancer statistics 2018: GLOBOCAN estimates of incidence and mortality worldwide for 36 cancers in 185 countries. *CA Cancer J Clin*, 68, 394-424.
- BREART, B., LEMAÎTRE, F., CELLI, S. & BOUSSO, P. 2008. Two-photon imaging of intratumoral CD8<sup>+</sup> T cell cytotoxic activity during adoptive T cell therapy in mice. *J Clin Invest*, 118, 1390-7.
- BROWN, C. E., BADIE, B., BARISH, M. E., WENG, L., OSTBERG, J. R., CHANG, W. C., NARANJO, A., STARR, R., WAGNER, J., WRIGHT, C., ZHAI, Y., BADING, J. R., RESSLER, J. A., PORTNOW, J., D'APUZZO, M., FORMAN, S. J. & JENSEN, M. C. 2015. Bioactivity and Safety of IL13R $\alpha$ 2-Redirected Chimeric Antigen Receptor CD8<sup>+</sup> T Cells in Patients with Recurrent Glioblastoma. *Clin Cancer Res*, 21, 4062-72.
- BULL, C., BOLTJE, T. J., BALNEGER, N., WEISCHER, S. M., WASSINK, M., VAN GEMST, J. J., BLOEMENDAL, V. R., BOON, L., VAN DER VLAG, J., HEISE, T., DEN BROK, M. H. & ADEMA, G. J. 2018. Sialic Acid Blockade Suppresses Tumor Growth by Enhancing T-cell-Mediated Tumor Immunity. *Cancer Res*, 78, 3574-3588.
- CADILHA, B. L., BENMEBAREK, M. R., DORMAN, K., ONER, A., LORENZINI, T., OBECK, H., VÄNTTINEN, M., DI PILATO, M., PRUESSMANN, J. N., STOIBER, S., HUYNH, D., MÄRKEL, F., SEIFERT, M., MANSKE, K., SUAREZ-GOSALVEZ, J., ZENG, Y., LESCH, S.,

- 
- KARCHES, C. H., HEISE, C., GOTTSCHLICH, A., THOMAS, M., MARR, C., ZHANG, J., PANDEY, D., FEUCHTINGER, T., SUBKLEWE, M., MEMPEL, T. R., ENDRES, S. & KOBOLD, S. 2021. Combined tumor-directed recruitment and protection from immune suppression enable CAR T cell efficacy in solid tumors. *Sci Adv*, 7.
- CHEADLE, E. J., SHEARD, V., ROTHWELL, D. G., BRIDGEMAN, J. S., ASHTON, G., HANSON, V., MANSOOR, A. W., HAWKINS, R. E. & GILHAM, D. E. 2014. Differential role of Th1 and Th2 cytokines in autotoxicity driven by CD19-specific second-generation chimeric antigen receptor T cells in a mouse model. *J Immunol*, 192, 3654-65.
- DONOVAN, L. K., DELAIDELLI, A., JOSEPH, S. K., BIELAMOWICZ, K., FOUSEK, K., HOLGADO, B. L., MANNO, A., SRIKANTHAN, D., GAD, A. Z., VAN OMMEREN, R., PRZELICKI, D., RICHMAN, C., RAMASWAMY, V., DANIELS, C., PALLOTA, J. G., DOUGLAS, T., JOYNT, A. C. M., HAAPASALO, J., NOR, C., VLADOIU, M. C., KUZAN-FISCHER, C. M., GARZIA, L., MACK, S. C., VARADHARAJAN, S., BAKER, M. L., HENDRIKSE, L., LY, M., KHARAS, K., BALIN, P., WU, X., QIN, L., HUANG, N., STUCKLIN, A. G., MORRISSY, A. S., CAVALLI, F. M. G., LUU, B., SUAREZ, R., DE ANTONELLIS, P., MICHEALRAJ, A., RASTAN, A., HEGDE, M., KOMOSA, M., SIRBU, O., KUMAR, S. A., ABDULLAEV, Z., FARIA, C. C., YIP, S., HUKIN, J., TABORI, U., HAWKINS, C., ALDAPE, K., DAUGAARD, M., MARIS, J. M., SORENSEN, P. H., AHMED, N. & TAYLOR, M. D. 2020. Locoregional delivery of CAR T cells to the cerebrospinal fluid for treatment of metastatic medulloblastoma and ependymoma. *Nat Med*, 26, 720-731.
- FENG, K., GUO, Y., DAI, H., WANG, Y., LI, X., JIA, H. & HAN, W. 2016. Chimeric antigen receptor-modified T cells for the immunotherapy of patients with EGFR-expressing advanced relapsed/refractory non-small cell lung cancer. *Sci China Life Sci*, 59, 468-79.
- FERLAY, J., COLOMBET, M., SOERJOMATARAM, I., MATHERS, C., PARKIN, D. M., PINEROS, M., ZNAOR, A. & BRAY, F. 2019. Estimating the global cancer incidence and mortality in 2018: GLOBOCAN sources and methods. *Int J Cancer*, 144, 1941-1953.
- FESNAK, A. D., JUNE, C. H. & LEVINE, B. L. 2016. Engineered T cells: the promise and challenges of cancer immunotherapy. *Nat Rev Cancer*, 16, 566-81.
- FOX, B. D., CHEUNG, V. J., PATEL, A. J., SUKI, D. & RAO, G. 2011. Epidemiology of metastatic brain tumors. *Neurosurg Clin N Am*, 22, 1-6, v.
- GAUTHIER, J. & TURTLE, C. J. 2021. Chimeric Antigen Receptor T-Cell Therapy for B-Cell Acute Lymphoblastic Leukemia: Current Landscape in 2021. *Cancer J*, 27, 98-106.
- GRIMM, J. B., ENGLISH, B. P., CHEN, J., SLAUGHTER, J. P., ZHANG, Z., REVYAKIN, A., PATEL, R., MACKLIN, J. J., NORMANNO, D., SINGER, R. H., LIONNET, T. & LAVIS, L. D. 2015. A general method to improve fluorophores for live-cell and single-molecule microscopy. *Nat Methods*, 12, 244-50, 3 p following 250.
- HARTMANN, J., SCHUSSLER-LENZ, M., BONDANZA, A. & BUCHHOLZ, C. J. 2017. Clinical development of CAR T cells-challenges and opportunities in translating innovative treatment concepts. *EMBO Mol Med*, 9, 1183-1197.

- 
- HAYDAR, D., HOUKE, H., CHIANG, J., YI, Z., ODÉ, Z., CALDWELL, K., ZHU, X., MERCER, K. S., STRIPAY, J. L., SHAW, T. I., VOGEL, P., DERENZO, C., BAKER, S. J., ROUSSEL, M. F., GOTTSCHALK, S. & KRENCIUTE, G. 2021. Cell-surface antigen profiling of pediatric brain tumors: B7-H3 is consistently expressed and can be targeted via local or systemic CAR T-cell delivery. *Neuro Oncol*, 23, 999-1011.
- HONG, G., DIAO, S., CHANG, J., ANTARIS, A. L., CHEN, C., ZHANG, B., ZHAO, S., ATOCHIN, D. N., HUANG, P. L., ANDREASSON, K. I., KUO, C. J. & DAI, H. 2014. Through-skull fluorescence imaging of the brain in a new near-infrared window. *Nat Photonics*, 8, 723-730.
- HORTON, K. L. & DWORKIN, S. L. 2013. Redefining gender-based power to move beyond interpersonal approaches to HIV prevention. *ANS Adv Nurs Sci*, 36, 42-50.
- HSU, P. C., TIAN, B., YANG, Y. L., WANG, Y. C., LIU, S., URISMAN, A., YANG, C. T., XU, Z., JABLONS, D. M. & YOU, L. 2019. Cucurbitacin E inhibits the Yes-associated protein signaling pathway and suppresses brain metastasis of human nonsmall cell lung cancer in a murine model. *Oncol Rep*, 42, 697-707.
- IRAGAVARAPU, C. & HILDEBRANDT, G. 2021. Lisocabtagene Maraleucel for the treatment of B-cell lymphoma. *Expert Opin Biol Ther*, 21, 1151-1156.
- IYER, A. K., SINGH, A., GANTA, S. & AMIJI, M. M. 2013. Role of integrated cancer nanomedicine in overcoming drug resistance. *Adv Drug Deliv Rev*, 65, 1784-802.
- JIN, L., TAO, H., KARACHI, A., LONG, Y., HOU, A. Y., NA, M., DYSON, K. A., GRIPPIN, A. J., DELEYROLLE, L. P., ZHANG, W., RAJON, D. A., WANG, Q. J., YANG, J. C., KRESAK, J. L., SAYOUR, E. J., RAHMAN, M., BOVA, F. J., LIN, Z., MITCHELL, D. A. & HUANG, J. 2019. CXCR1- or CXCR2-modified CAR T cells co-opt IL-8 for maximal antitumor efficacy in solid tumors. *Nat Commun*, 10, 4016.
- JOHNSON, L. R., LEE, D. Y., EACRET, J. S., YE, D., JUNE, C. H. & MINN, A. J. 2021. The immunostimulatory RNA RN7SL1 enables CAR-T cells to enhance autonomous and endogenous immune function. *Cell*, 184, 4981-4995 e14.
- KAECH, S. M. & AHMED, R. 2001. Memory CD8+ T cell differentiation: initial antigen encounter triggers a developmental program in naive cells. *Nat Immunol*, 2, 415-22.
- KALKANIS, S. N. & LINSKEY, M. E. 2010. Evidence-based clinical practice parameter guidelines for the treatment of patients with metastatic brain tumors: introduction. *J Neurooncol*, 96, 7-10.
- KARCHES, C. H., BENMEBAREK, M. R., SCHMIDBAUER, M. L., KURZAY, M., KLAUS, R., GEIGER, M., RATAJ, F., CADILHA, B. L., LESCH, S., HEISE, C., MURR, R., VOM BERG, J., JASTROCH, M., LAMP, D., DING, J., DUEWELL, P., NIEDERFELLNER, G., SUSTMANN, C., ENDRES, S., KLEIN, C. & KOBOLD, S. 2019. Bispecific Antibodies Enable Synthetic Agonistic Receptor-Transduced T Cells for Tumor Immunotherapy. *Clin Cancer Res*, 25, 5890-5900.
- KARSCHNIA, P., TESKE, N., THON, N., SUBKLEWE, M., TONN, J. C., DIETRICH, J. & VON

- 
- BAUMGARTEN, L. 2021. Chimeric Antigen Receptor T Cells for Glioblastoma: Current Concepts, Challenges, and Future Perspectives. *Neurology*, 97, 218-230.
- KIENAST, Y., VON BAUMGARTEN, L., FUHRMANN, M., KLINKERT, W. E., GOLDBRUNNER, R., HERMS, J. & WINKLER, F. 2010. Real-time imaging reveals the single steps of brain metastasis formation. *Nat Med*, 16, 116-22.
- KIM, M. K., SHIN, S. J., LEE, H. M., CHOI, H. S., JEONG, J., KIM, H., PAIK, S. S., KIM, M., CHOI, D. & RYU, C. J. 2019. Mycoplasma infection promotes tumor progression via interaction of the mycoplasmal protein p37 and epithelial cell adhesion molecule in hepatocellular carcinoma. *Cancer Lett*, 454, 44-52.
- KIM, Y., KIM, H. S., CUI, Z. Y., LEE, H. S., AHN, J. S., PARK, C. K., PARK, K. & AHN, M. J. 2009. Clinicopathological implications of EpCAM expression in adenocarcinoma of the lung. *Anticancer Res*, 29, 1817-22.
- KOBAT, D., DURST, M. E., NISHIMURA, N., WONG, A. W., SCHAFFER, C. B. & XU, C. 2009. Deep tissue multiphoton microscopy using longer wavelength excitation. *Opt Express*, 17, 13354-64.
- LEE, J. & AHN, M. J. 2021. Brain metastases in patients with oncogenic-driven non-small cell lung cancer: Pros and cons for early radiotherapy. *Cancer Treat Rev*, 100, 102291.
- LESCH, S., BLUMENBERG, V., STOIBER, S., GOTTSCHLICH, A., OGONEK, J., CADILHA, B. L., DANTES, Z., RATAJ, F., DORMAN, K., LUTZ, J., KARCHES, C. H., HEISE, C., KURZAY, M., LARIMER, B. M., GRASSMANN, S., RAPP, M., NOTTEBROCK, A., KRUGER, S., TOKAREW, N., METZGER, P., HOERTH, C., BENMEBAREK, M. R., DHOQINA, D., GRÜNMEIER, R., SEIFERT, M., OENER, A., UMUT, Ö., JOAQUINA, S., VIMEUX, L., TRAN, T., HANK, T., BABA, T., HUYNH, D., MEGENS, R. T. A., JANSSEN, K. P., JASTROCH, M., LAMP, D., RUEHLAND, S., DI PILATO, M., PRUESSMANN, J. N., THOMAS, M., MARR, C., ORMANN, S., REISCHER, A., HRISTOV, M., TARTOUR, E., DONNADIEU, E., ROTHENFUSSER, S., DUEWELL, P., KÖNIG, L. M., SCHNURR, M., SUBKLEWE, M., LISS, A. S., HALAMA, N., REICHERT, M., MEMPEL, T. R., ENDRES, S. & KOBOLD, S. 2021. T cells armed with C-X-C chemokine receptor type 6 enhance adoptive cell therapy for pancreatic tumours. *Nat Biomed Eng*, 5, 1246-1260.
- LI, H., HUANG, Y., JIANG, D. Q., CUI, L. Z., HE, Z., WANG, C., ZHANG, Z. W., ZHU, H. L., DING, Y. M., LI, L. F., LI, Q., JIN, H. J. & QIAN, Q. J. 2018. Antitumor activity of EGFR-specific CAR T cells against non-small-cell lung cancer cells in vitro and in mice. *Cell Death Dis*, 9, 177.
- LI, W., ZHOU, Y., WU, Z., SHI, Y., TIAN, E., ZHU, Y., WANG, T., DOU, W., MENG, X., CHEN, M., ZHAI, B. & ZHU, D. 2021. Targeting Wnt Signaling in the Tumor Immune Microenvironment to Enhancing EpCAM CAR T-Cell therapy. *Front Pharmacol*, 12, 724306.
- MAJ, T., WANG, W., CRESPO, J., ZHANG, H., WANG, W., WEI, S., ZHAO, L., VATAN, L., SHAO, I., SZELIGA, W., LYSSIOTIS, C., LIU, J. R., KRYCZEK, I. & ZOU, W. 2017. Oxidative stress controls regulatory T cell apoptosis and suppressor activity and PD-L1-blockade

- 
- resistance in tumor. *Nat Immunol*, 18, 1332-1341.
- MASUDA, C., SUGIMOTO, M., WAKITA, D., MONNAI, M., ISHIMARU, C., NAKAMURA, R., KINOSHITA, M., YOROZU, K., KURASAWA, M., KONDOH, O. & YAMAMOTO, K. 2020. Bevacizumab suppresses the growth of established non-small-cell lung cancer brain metastases in a hematogenous brain metastasis model. *Clin Exp Metastasis*, 37, 199-207.
- MIAO, C. C., HWANG, W., CHU, L. Y., YANG, L. H., HA, C. T., CHEN, P. Y., KUO, M. H., LIN, S. C., YANG, Y. Y., CHUANG, S. E., YU, C. C., PAN, S. T., KAO, M. C., CHANG, C. R. & CHOU, Y. T. 2022. LC3A-mediated autophagy regulates lung cancer cell plasticity. *Autophagy*, 18, 921-934.
- MISGELD, T. & KERSCHENSTEINER, M. 2006. In vivo imaging of the diseased nervous system. *Nat Rev Neurosci*, 7, 449-63.
- MOIN, A. T., SARKAR, B., ULLAH, M. A., ARAF, Y., AHMED, N. & RUDRA, B. 2021. In silico assessment of EpCAM transcriptional expression and determination of the prognostic biomarker for human lung adenocarcinoma (LUAD) and lung squamous cell carcinoma (LUSC). *Biochem Biophys Rep*, 27, 101074.
- MOLDENHAUER, G., SALNIKOV, A. V., LUTTGAU, S., HERR, I., ANDERL, J. & FAULSTICH, H. 2012. Therapeutic potential of amanitin-conjugated anti-epithelial cell adhesion molecule monoclonal antibody against pancreatic carcinoma. *J Natl Cancer Inst*, 104, 622-34.
- MULAZZANI, M., FRASSLE, S. P., VON MUCKE-HEIM, I., LANGER, S., ZHOU, X., ISHIKAWA-ANKERHOLD, H., LEUBE, J., ZHANG, W., DOTSCH, S., SVEC, M., RUDELIUS, M., DREYLING, M., VON BERGWELT-BAILDON, M., STRAUBE, A., BUCHHOLZ, V. R., BUSCH, D. H. & VON BAUMGARTEN, L. 2019. Long-term in vivo microscopy of CAR T cell dynamics during eradication of CNS lymphoma in mice. *Proc Natl Acad Sci U S A*, 116, 24275-24284.
- NGUYEN, Q. T., CALLAMARAS, N., HSIEH, C. & PARKER, I. 2001. Construction of a two-photon microscope for video-rate Ca(2+) imaging. *Cell Calcium*, 30, 383-93.
- PAGE, S., MILNER-WATTS, C., PERNA, M., JANZIC, U., VIDAL, N., KAUDEER, N., AHMED, M., MCDONALD, F., LOCKE, I., MINCHOM, A., BHOSLE, J., WELSH, L. & O'BRIEN, M. 2020. Systemic treatment of brain metastases in non-small cell lung cancer. *Eur J Cancer*, 132, 187-198.
- PATRIARCA, C., MACCHI, R. M., MARSCHNER, A. K. & MELLSTEDT, H. 2012. Epithelial cell adhesion molecule expression (CD326) in cancer: a short review. *Cancer Treat Rev*, 38, 68-75.
- PECHOUX, C. L., DHERMAIN, F. & BESSE, B. 2016. Whole brain radiotherapy in patients with NSCLC and brain metastases. *Lancet*, 388, 1960-1962.
- PÉREZ-ALVAREZ, A., ARAQUE, A. & MARTÍN, E. D. 2013. Confocal microscopy for astrocyte in vivo imaging: Recycle and reuse in microscopy. *Front Cell Neurosci*, 7, 51.

- 
- PRICEMAN, S. J., TILAKAWARDANE, D., JEANG, B., AGUILAR, B., MURAD, J. P., PARK, A. K., CHANG, W. C., OSTBERG, J. R., NEMAN, J., JANDIAL, R., PORTNOW, J., FORMAN, S. J. & BROWN, C. E. 2018. Regional Delivery of Chimeric Antigen Receptor-Engineered T Cells Effectively Targets HER2(+) Breast Cancer Metastasis to the Brain. *Clin Cancer Res*, 24, 95-105.
- RAFIQ, S., HACKETT, C. S. & BRENTJENS, R. J. 2020. Engineering strategies to overcome the current roadblocks in CAR T cell therapy. *Nat Rev Clin Oncol*, 17, 147-167.
- RAMIREZ, A. G. & TRAPIDO, E. J. 2020. Advancing the Science of Cancer in Latinos. In: RAMIREZ, A. G. & TRAPIDO, E. J. (eds.) *Advancing the Science of Cancer in Latinos*. Cham (CH).
- REPPEL, L., TSAHOURIDIS, O., AKULIAN, J., DAVIS, I. J., LEE, H., FUCA, G., WEISS, J., DOTTI, G., PECOT, C. V. & SAVOLDO, B. 2022. Targeting disialoganglioside GD2 with chimeric antigen receptor-redirected T cells in lung cancer. *J Immunother Cancer*, 10.
- RESHAK, A. H. 2008. Reduction of the pulse duration of the ultrafast laser pulses of the Two-Photon Laser Scanning Microscopy (2PLSM). *BMC Res Notes*, 1, 39.
- RESHAK, A. H. 2009. Second harmonic generation from thick leaves using the two-photon laser scanning microscope. *Micron*, 40, 455-62.
- RUSTHOVEN, C. G., YAMAMOTO, M., BERNHARDT, D., SMITH, D. E., GAO, D., SERIZAWA, T., YOMO, S., AIYAMA, H., HIGUCHI, Y., SHUTO, T., AKABANE, A., SATO, Y., NIRANJAN, A., FARAMAND, A. M., LUNSFORD, L. D., MCINERNEY, J., TUANQUIN, L. C., ZACHARIA, B. E., CHIANG, V., SINGH, C., YU, J. B., BRAUNSTEIN, S., MATHIEU, D., TOUCHETTE, C. J., LEE, C. C., YANG, H. C., AIZER, A. A., CAGNEY, D. N., CHAN, M. D., KONDZIOLKA, D., BERNSTEIN, K., SILVERMAN, J. S., GRILLS, I. S., SIDDIQUI, Z. A., YUAN, J. C., SHEEHAN, J. P., CORDEIRO, D., NOSAKI, K., SETO, T., DEIBERT, C. P., VERMA, V., DAY, S., HALASZ, L. M., WARNICK, R. E., TRIFILETTI, D. M., PALMER, J. D., ATTIA, A., LI, B., CIFARELLI, C. P., BROWN, P. D., VARGO, J. A., COMBS, S. E., KESSEL, K. A., RIEKEN, S., PATEL, S., GUCKENBERGER, M., ANDRATSCHKE, N., KAVANAGH, B. D. & ROBIN, T. P. 2020. Evaluation of First-line Radiosurgery vs Whole-Brain Radiotherapy for Small Cell Lung Cancer Brain Metastases: The FIRE-SCLC Cohort Study. *JAMA Oncol*, 6, 1028-1037.
- SAMPSON, J. H., CHOI, B. D., SANCHEZ-PEREZ, L., SURYADEVARA, C. M., SNYDER, D. J., FLORES, C. T., SCHMITTLING, R. J., NAIR, S. K., REAP, E. A., NORBERG, P. K., HERNDON, J. E., 2ND, KUAN, C. T., MORGAN, R. A., ROSENBERG, S. A. & JOHNSON, L. A. 2014. EGFRvIII mCAR-modified T-cell therapy cures mice with established intracerebral glioma and generates host immunity against tumor-antigen loss. *Clin Cancer Res*, 20, 972-84.
- SHAW, A. T., BAUER, T. M., DE MARINIS, F., FELIP, E., GOTO, Y., LIU, G., MAZIERES, J., KIM, D. W., MOK, T., POLLI, A., THURM, H., CALELLA, A. M., PELTZ, G. & SOLOMON, B. J. 2020. First-Line Lorlatinib or Crizotinib in Advanced ALK-Positive Lung Cancer. *N Engl J Med*, 383, 2018-2029.

- 
- SHIINA, S., OHNO, M., OHKA, F., KURAMITSU, S., YAMAMICHI, A., KATO, A., MOTOMURA, K., TANAHASHI, K., YAMAMOTO, T., WATANABE, R., ITO, I., SENGA, T., HAMAGUCHI, M., WAKABAYASHI, T., KANEKO, M. K., KATO, Y., CHANDRAMOHAN, V., BIGNER, D. D. & NATSUME, A. 2016. CAR T Cells Targeting Podoplanin Reduce Orthotopic Glioblastomas in Mouse Brains. *Cancer Immunol Res*, 4, 259-68.
- SHYER, J. A., FLAVELL, R. A. & BAILIS, W. 2020. Metabolic signaling in T cells. *Cell Res*, 30, 649-659.
- SIEGEL, R. L., MILLER, K. D. & JEMAL, A. 2020. Cancer statistics, 2020. *CA Cancer J Clin*, 70, 7-30.
- SIMON, M., STEFAN, N., PLUCKTHUN, A. & ZANGEMEISTER-WITTKE, U. 2013. Epithelial cell adhesion molecule-targeted drug delivery for cancer therapy. *Expert Opin Drug Deliv*, 10, 451-68.
- SON, J., CHO, J. W., PARK, H. J., MOON, J., PARK, S., LEE, H., LEE, J., KIM, G., PARK, S. M., LIRA, S. A., MCKENZIE, A. N., KIM, H. Y., CHOI, C. Y., LIM, Y. T., PARK, S. Y., KIM, H. R., PARK, S. H., SHIN, E. C., LEE, I. & HA, S. J. 2020. Tumor-Infiltrating Regulatory T-cell Accumulation in the Tumor Microenvironment Is Mediated by IL33/ST2 Signaling. *Cancer Immunol Res*, 8, 1393-1406.
- SPIZZO, G., FONG, D., WURM, M., ENSINGER, C., OBRIST, P., HOFER, C., MAZZOLENI, G., GASTL, G. & WENT, P. 2011. EpCAM expression in primary tumour tissues and metastases: an immunohistochemical analysis. *J Clin Pathol*, 64, 415-20.
- SUNG, H., FERLAY, J., SIEGEL, R. L., LAVERSANNE, M., SOERJOMATARAM, I., JEMAL, A. & BRAY, F. 2021. Global Cancer Statistics 2020: GLOBOCAN Estimates of Incidence and Mortality Worldwide for 36 Cancers in 185 Countries. *CA Cancer J Clin*, 71, 209-249.
- TOTH, G., SZOLLOSI, J., ABKEN, H., VEREB, G. & SZOOR, A. 2020. A Small Number of HER2 Redirected CAR T Cells Significantly Improves Immune Response of Adoptively Transferred Mouse Lymphocytes against Human Breast Cancer Xenografts. *Int J Mol Sci*, 21.
- TRZPIS, M., MCLAUGHLIN, P. M., DE LEIJ, L. M. & HARMSSEN, M. C. 2007. Epithelial cell adhesion molecule: more than a carcinoma marker and adhesion molecule. *Am J Pathol*, 171, 386-95.
- UPADHYAY, R., BOIARSKY, J. A., PANTSULAIA, G., SVENSSON-ARVELUND, J., LIN, M. J., WROBLEWSKA, A., BHALLA, S., SCHOLLER, N., BOT, A., ROSSI, J. M., SADEK, N., PAREKH, S., LAGANA, A., BACCARINI, A., MERAD, M., BROWN, B. D. & BRODY, J. D. 2021. A Critical Role for Fas-Mediated Off-Target Tumor Killing in T-cell Immunotherapy. *Cancer Discov*, 11, 599-613.
- VALIENTE, M., AHLUWALIA, M. S., BOIRE, A., BRASTIANOS, P. K., GOLDBERG, S. B., LEE, E. Q., LE RHUN, E., PREUSSER, M., WINKLER, F. & SOFFIETTI, R. 2018. The Evolving Landscape of Brain Metastasis. *Trends Cancer*, 4, 176-196.
- VARGO, M. M. 2017. Brain Tumors and Metastases. *Phys Med Rehabil Clin N Am*, 28,

- VON BAUMGARTEN, L., BRUCKER, D., TIRNICERU, A., KIENAST, Y., GRAU, S., BURGOLD, S., HERMS, J. & WINKLER, F. 2011. Bevacizumab has differential and dose-dependent effects on glioma blood vessels and tumor cells. *Clin Cancer Res*, 17, 6192-205.
- WALLSTABE, L., GOTTLICH, C., NELKE, L. C., KUHNEMUNDT, J., SCHWARZ, T., NERRETER, T., EINSELE, H., WALLE, H., DANDEKAR, G., NIETZER, S. L. & HUDECEK, M. 2019. ROR1-CAR T cells are effective against lung and breast cancer in advanced microphysiologic 3D tumor models. *JCI Insight*, 4.
- WANG, D., STARR, R., CHANG, W. C., AGUILAR, B., ALIZADEH, D., WRIGHT, S. L., YANG, X., BRITO, A., SARKISSIAN, A., OSTBERG, J. R., LI, L., SHI, Y., GUTOVA, M., ABOODY, K., BADIE, B., FORMAN, S. J., BARISH, M. E. & BROWN, C. E. 2020. Chlorotoxin-directed CAR T cells for specific and effective targeting of glioblastoma. *Sci Transl Med*, 12.
- WANG, X., HUYNH, C., URAK, R., WENG, L., WALTER, M., LIM, L., VYAS, V., CHANG, W. C., AGUILAR, B., BRITO, A., SARKISSIAN, A., BANDARA, N. A., YANG, L., WANG, J., WU, X., ZHANG, J., PRICEMAN, S. J., QIN, H., KWAK, L. W., BUDDE, L. E., THOMAS, S. H., CLARK, M. C., POPPLEWELL, L., SIDDIQI, T., BROWN, C. E. & FORMAN, S. J. 2021. The Cerebroventricular Environment Modifies CAR T Cells for Potent Activity against Both Central Nervous System and Systemic Lymphoma. *Cancer Immunol Res*, 9, 75-88.
- WEISS, T., WELLER, M., GUCKENBERGER, M., SENTMAN, C. L. & ROTH, P. 2018. NKG2D-Based CAR T Cells and Radiotherapy Exert Synergistic Efficacy in Glioblastoma. *Cancer Res*, 78, 1031-1043.
- WILLIAMS, P. S., MOORE, L. R., JOSHI, P., GOODIN, M., ZBOROWSKI, M. & FLEISCHMAN, A. 2021. Microfluidic chip for graduated magnetic separation of circulating tumor cells by their epithelial cell adhesion molecule expression and magnetic nanoparticle binding. *J Chromatogr A*, 1637, 461823.
- YANG, J., ISAJI, T., ZHANG, G., QI, F., DUAN, C., FUKUDA, T. & GU, J. 2020. EpCAM associates with integrin and regulates cell adhesion in cancer cells. *Biochem Biophys Res Commun*, 522, 903-909.
- YEKU, O., LI, X. & BRENTJENS, R. J. 2017. Adoptive T-Cell Therapy for Solid Tumors. *Am Soc Clin Oncol Educ Book*, 37, 193-204.
- YOUSEFI, M., BAHRAMI, T., SALMANINEJAD, A., NOSRATI, R., GHAFFARI, P. & GHAFFARI, S. H. 2017. Lung cancer-associated brain metastasis: Molecular mechanisms and therapeutic options. *Cell Oncol (Dordr)*, 40, 419-441.
- YUN, M. R., KIM, D. H., KIM, S. Y., JOO, H. S., LEE, Y. W., CHOI, H. M., PARK, C. W., HEO, S. G., KANG, H. N., LEE, S. S., SCHOENFELD, A. J., DRILON, A., KANG, S. G., SHIM, H. S., HONG, M. H., CUI, J. J., KIM, H. R. & CHO, B. C. 2020. Repotrectinib Exhibits Potent Antitumor Activity in Treatment-Naive and Solvent-Front-Mutant ROS1-Rearranged Non-Small Cell Lung Cancer. *Clin Cancer Res*, 26, 3287-3295.

---

ZHANG, W., KARSCHNIA, P., VON MUCKE-HEIM, I. A., MULAZZANI, M., ZHOU, X., BLOBNER, J., MUELLER, N., TESKE, N., DEDE, S., XU, T., THON, N., ISHIKAWA-ANKERHOLD, H., STRAUBE, A., TONN, J. C. & VON BAUMGARTEN, L. 2021. In vivo two-photon characterization of tumor-associated macrophages and microglia (TAM/M) and CX3CR1 during different steps of brain metastasis formation from lung cancer. *Neoplasia*, 23, 1089-1100.

ZIPFEL, W. R., WILLIAMS, R. M. & WEBB, W. W. 2003. Nonlinear magic: multiphoton microscopy in the biosciences. *Nat Biotechnol*, 21, 1369-77.

---

## 7. Acknowledgement

Time flies, my slightly long and tortuous doctoral career is coming to an end. I spent the most unforgettable four years of my life at the University of Munich, and I also showed my youth and enthusiasm in these four years. Along the way, there are too many things I want to say, and there are too many people I want to thank. My supervisor, colleagues, relatives and friends, it is your help and care in all aspects that enable me to persevere all the way. With your company, my academic career is full of brilliant colors.

My supervisor (Louisa von Baumgarten) has devoted a lot of hard work to my thesis. From the topic selection and implementation of the thesis to the finalization of the final paper, she has provided me with careful guidance and all-round support. Over four years, she had devoted themselves to the academic guidance and strict requirements on the work. Her extensive professional knowledge, rigorous academic attitude, selfless work spirit, and honest demeanor have benefited me a lot, and those will surely benefit me throughout my life. Here, I would like to extend my highest respect and heartfelt thanks to her!

During the M.D. study, Prof. Massberg, Prof. Straube and Matthias Mulazzani put forward many valuable suggestions on my project research plan, the specific implementation of the research work, the difficulties encountered in the experiment process, and the writing of the thesis, which contributed to the smooth development and completion of my thesis. I hereby express my heartfelt gratitude! The successful completion of this thesis is also inseparable from the great help and support of Prof. Sebastian Kobold and postdoc Bruno L. Cadilha. They gave guidance on the topic selection and development of the thesis, and I would like to

---

express my gratitude!

Most of the work in this thesis was completed in the Walter Brendel Center. During the experiment, I received great help and support from Prof. Schulz, Michael Lorenz, Susanne, Anna, Hellen and Dominic. And many thanks to Zhe Zhang, Shuxia Fan and Wenlong Zhang for my guidance in scientific research. Thanks to Sigrid Langer and Sertac Dede for their great help in study and life.

Here, I would also like to thank my family. You unconditionally supported any decision I made along the way and gave me all the love you could give, especially my old sister, who took most of the family responsibilities for me.

In front of my heart, the language is so pale. Finally, with my sincere heart, I would like to thank all the teachers, colleagues and friends who have not mentioned here and who have cared and helped me! Thank you for your support, encouragement, care and company, and sincerely wish my loved ones and those who love me all the best in their future life!

---

## 8. Affidavit



### Affidavit

Xu, Tao

Surname, first name

Street

Zip code, town, country

I hereby declare, that the submitted thesis entitled:

EpCAM CAR T cells for the treatment of lung cancer brain metastasis- an in vivo imaging study in the mouse

is my own work. I have only used the sources indicated and have not made unauthorized use of services of a third party. Where the work of others has been quoted or reproduced, the source is always given.

I further declare that the submitted thesis or parts thereof have not been presented as part of an examination degree to any other university.

Munich, 03.11.2022

Place, date

Tao Xu

Signature doctoral candidate